The Middle Stone Age Sequence at Klipfonteinrand 1 (KFR1), Western Cape, South Africa

Alex Mackay[1,2,3] · Rosaria B. K. Saktura[1] · Corey A. O'Driscoll[1] ·
Kelsey C. Boyd[1] · Ben Marwick[4] · Ian Moffat[5] · Zenobia Jacobs[1,3]

Abstract

The rock shelter site Klipfonteinrand 1 (KFR1), located on the edge of southern Africa's Fynbos biome, was initially excavated by John Parkington in 1969. Due to difficulties resolving the stratigraphic sequence, the lack of age estimates, and generally poor organic preservation, the Middle Stone Age (MSA) components of the site have received limited attention. In this paper we report on the re-excavation, dating, palaeoecology, and cultural sequence recovered from a trench placed adjacent to Parkington's original excavation. The refined sequence includes three stratigraphically distinct MSA components: a Howiesons Poort component dating to ~69 ka, and two earlier MSA components dating to ~85 ka and ~156 ka. These are overlain by two younger components dated to the late Pleistocene and early Holocene. Bedrock morphology at the site is complex, and the oldest component appears to be restricted to a small area of relatively deep (1.9 m) sediment accumulation towards the centre of the sheltered area. Phytoliths suggest limited change in floral communities near the site across the lowest three units—which include parts of marine isotope stages (MIS) 6, 5, and 4—reflecting the characteristic stability of the Fynbos biome. The stone artefacts in the oldest MSA component include large blades that are absent from the overlying strata, and that may be a distinct element of late MIS 6 technology in the area. Interestingly, neither the early MSA nor early Holocene components we describe here were encountered in the rear trench at the site, 3 m away, which instead produced a sequence dominated by marine isotope stage 2 occupation. KFR1 presents new insights into the archaeology of the earlier MSA in southern Africa, while also providing a cautionary note on the discontinuous and spatially variable nature of rock shelter occupation in the region.

Keywords Middle Stone Age · Southern Africa · Lithics · OSL dating · Phytoliths · Geoarchaeology · Remote sensing

Introduction

Archaeological evidence from the southern African Middle Stone Age (MSA) has been instrumental in over-turning long held assumptions about human behavioural evolution, suggesting a deeper antiquity to a range of novel behaviours than had previously been expected (Wadley, 2015, Scerri and Will, 2023, Henshilwood, 2012). Though the later phases of the MSA are—with important exceptions (Will and Conard, 2018, Mitchell, 2008)—increasingly well understood, there is a need to improve our understanding of the earlier MSA between the first documented appearance of our species ~300 ka (Richter et al., 2017), and the relatively well-resolved southern African record post-dating ~75 ka (Mackay et al., 2014). Complicating this is the fact that many key early MSA sites were excavated decades ago and have not since been re-excavated or dated (Morrissey et al., 2022). This problem exacerbates the inevitable tendency for older sites to be less common than younger sites, leading to sparse and poorly constrained coverage of the archaeology of marine isotope stages (MIS) 5–8 (Chazan et al., 2020).

Situated in the Western Cape of South Africa, the rock shelter site Klipfonteinrand 1 (hereafter KFR1) is an iconic but problematic MSA site known for its Holocene Later Stone Age (LSA) burials, Howiesons Poort, and earlier MSA stone artefact assemblages (Volman, 1981, Parkington, 1980, Henshilwood, 2012). The site was originally excavated by John Parkington in 1969, but detailed results of that excavation were never published, and the MSA components of the site remained undated. In spite of this, the MSA artefact assemblage formed part of Volman's influential southern African MSA technological synthesis (Volman, 1981).

Volman identified Howiesons Poort material in the upper MSA at KFR1, while artefacts in the lower deposits were assigned to his MSA 2b unit. Complicating his analysis was cross-cutting of strata during Parkington's excavation (Volman, 1981), resulting from variable depositional planes and the ambiguity of stratigraphy (see below). Mixing occurred between LSA and MSA assemblages, as well as between the two identified MSA components. Furthermore, the original excavation only extended to bedrock in one area, reducing Volman's sample of the earliest material at the site.

We re-excavated KFR1 in 2011 and 2012. Two trenches were excavated to bedrock, one towards the front of the shelter in the area of Parkington's original deep sounding, and another towards the rear wall in an area that had not previously been excavated. Reinforcing the complex occupational and depositional sequence at the site, the rear trench produced a sequence spanning approximately 23–13 ka and comprising cultural components (Robberg and Oakhurst) not encountered in excavations towards the front (Mackay et al., 2019).

In the present paper we describe the excavation, stratigraphy, dating, and palaeoecology from the front trench at the site. We also discuss the results of geochemical and geophysical work which helps to explain patterns of deposit depth and age. Using single-grain optically stimulated luminescence (OSL) dating of quartz, we differentiate three MSA occupation pulses in the front trench at ~156
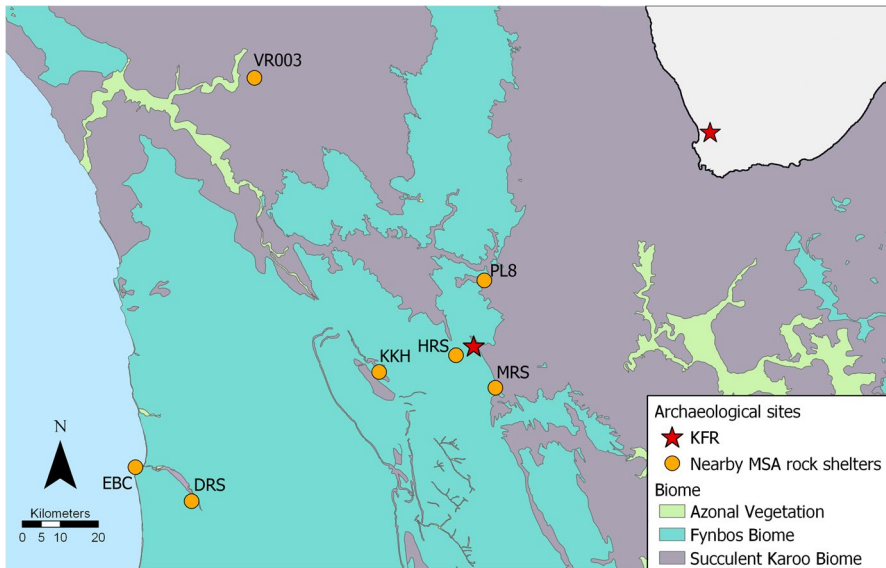
Fig. 1 Study area with vegetation biomes and nearby MSA rock shelter sites, both dated and undated. Inset shows location of study area in southern Africa. Site abbreviations as follows: DRS Diepkloof, EBC Elands Bay Cave, HRS Hollow Rock Shelter, KKH Klein Kliphuis, MRS Mertenhof Rock Shelter, PL8 Putslaagte 8, VR003 Varsche Rivier 003. Vegetation data from Mucina and Rutherford (2006)

ka, ~85 ka, and ~69 ka. These are capped by sediments and artefacts deposited ~11–8 ka, a component not detected at the rear of the cave.

KFR1 preserves an unexpectedly old MSA assemblage, extending into MIS 6. Our results also attest to both the episodic nature of rock shelter occupation in the region, and the consequent patchiness of the earlier MSA record. The lack of sites near KFR1 with ages consistent with the oldest occupation pulse highlights the difficulty of interrogating human behavioural evolution during this critical period.

Location and Excavation History of Klipfonteinrand 1 Rock Shelter

KFR1 is a prominent north-east facing rock shelter located in the rain-shadow side of the Cederberg Mountains, 78 km east of the present day coastline and around 200 km north of Cape Town (Fig. 1). The surrounding vegetation is Cederberg Sandstone Fynbos (Mucina and Rutherford, 2006), though the boundary with the Succulent Karoo biome lies only 400 m east of the site. This boundary partly reflects edaphic controls relating to the shift from Nardouw Formation sandstones (upper Table Mountain Group)—in which KFR1 was formed—to the overlying Ceres Formation shales (lower Bokkeveld Group).

KFR1 is one of a cluster of MSA sites in this area, the nearest being Hollow Rock Shelter, located 2 km to the west (Evans, 1994). Those dated to MIS 4 include Diepkloof, Hollow Rock Shelter, Klein Kliphuis, Putslaagte 8, and Varsche Rivier 003, all of which have Howiesons Poort, Still Bay, or both components (Jacobs et al.,
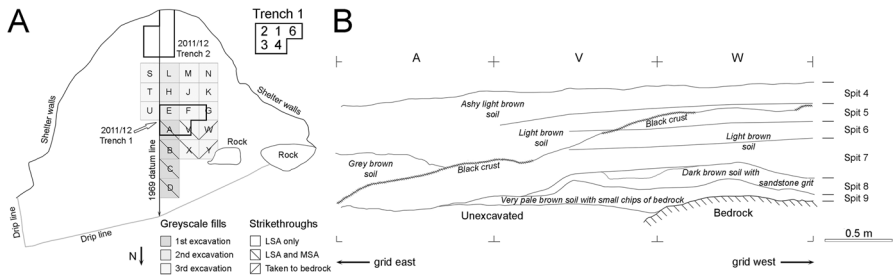
Fig. 2 (**A**) Plan of Parkington's 1969 excavation at KFR1 with location of 2011–2012 trenches also shown. A inset shows squares numbers for 2011/12 excavation of Trench 1. (**B**) The south section of Parkington's deep sounding along the AVW line

2008, Jacobs and Roberts, 2015, Mackay et al., 2015, Högberg, 2014, Mackay et al., 2022b). Diepkloof, Elands Bay Cave, Hollow Rock Shelter, and Varsche Rivier 003 also contain deposits dated to MIS 5 (Högberg, 2014, Jacobs and Roberts, 2015, Tribolo et al., 2016, Mackay et al., 2022a), though the MIS 5 ages at Hollow Rock Shelter are derived from Still Bay deposits. Elands Bay Cave is the only site in the region with pre-MIS 5 deposits—a single age estimate of 236 ± 23 ka from layer Liam (Tribolo et al., 2016).

KFR1 was reported by Hyme Rabinowitz and colleagues following rock art surveys in 1961 and excavated by John Parkington in three visits between September and December 1969. Parkington opened a total of twenty 1.22 m (four foot) squares in the central part of the shelter (Fig. 2A). Excavation in twelve squares was discontinued while still within the LSA; six continued into the MSA, and two were taken down to bedrock. The results of these excavations were never published, though they produced two undergraduate theses (Thackeray, 1977, Nackerdien, 1989) and contributed to two PhD theses (Mackay, 2009, Parkington, 1977). The excavation can be reconstructed from those works in combination with Parkington's unpublished field diary.

The sheltered area at KFR1 covers 162.7 m^2, measuring 13.5 m from the dripline to the rear wall and 18 m across the mouth (Fig. 3C). At its highest point the shelter measures 6 m from the top of the deposit to the ceiling. The current surface of the deposit at KFR1 is loose and sandy, and exhibits a significant slope from the south west (rear west) corner to the north east corner of the shelter mouth. The site was actively used as a kraal (animal pen) prior to and after Parkington's excavation.

The first phase of Parkington's excavation focussed on four squares denoted A through D along the main datum line (Fig. 2A). Excavation units initially followed visible stratigraphy and depositional features such as dung crusts and intermittent ash units, below which the excavators encountered a 'clayey brown soil' unit that was removed in 5–6 inch (~127–154 mm) spits following the slope of the surface deposits. The undifferentiated nature of the sedimentary deposits through the upper 500 mm of Square A prompted Parkington to query in his excavation diary: "will the brown clayey soil ever end?" (24 September 1969). Later noting the lack of 'apparent structure to the soil' and the absence of indicators to the 'dip and strike of the
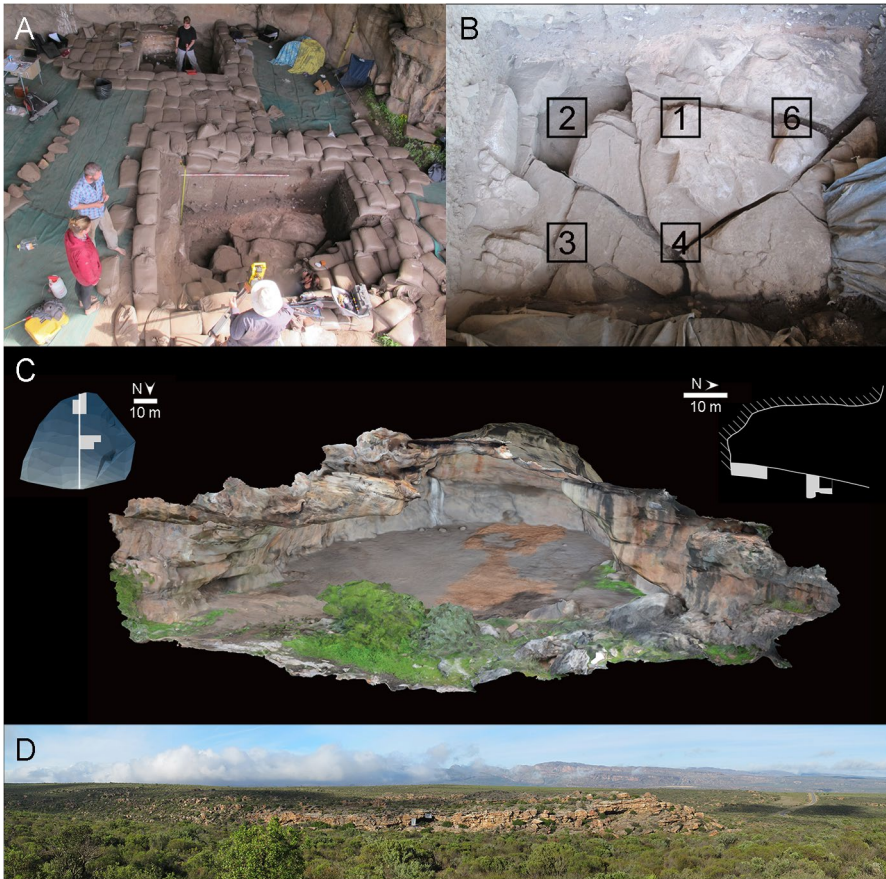
Fig. 3 (**A**) Overview of excavation at KFR1 during 2012 showing both Trench 1 (front) and Trench 2 (rear). (**B**) Layout of squares in Trench 1. (**C**) 3D photomosaic of KFR1 after backfill. [Inset top left] Plan view of site with trenches indicated and slope shown as shaded 0.1 m elevation bands (darker is higher). [Inset top right] Section view through the cave showing location of trenches relative to slope of deposit. Note that bedrock was reached in both trenches. (**D**) Panorama of KFR1 with sunshades up looking west towards the Cederberg

deposit', Parkington concluded, correctly: "This will be a problem" (26 September 1969). Around the contact between spits 3 and 4, the excavators noted the appearance of large quartzite flakes with faceted platforms, suggesting the transition from LSA to MSA material.

Other than some variation in grit, the only apparent stratigraphic indicator within Parkington's brown clayey soil was a discontinuous 'black breccia crust' which in places indicated flat depositional planes and in other places a steep slope to the north east (Fig. 2B). Notably, though the brown soil was identified both above and below the black crust, bone was largely absent beneath it, and MSA artefacts became more common.

Table 1 Existing radiocarbon dates from 1969 and 2011–2012 excavation at KFR1

Excavation	Trench	Stratum	Technique	Lab code	Uncalibrated age	Calibrated age
Parkington	n/a	Spit1	14C	Pta-1642	3540 ± 60	3593-3971
Parkington	n/a	HAS1	14C	Pta-2476	5570 ± 70	6195-6488
Parkington	n/a	Spit3	14C	Pta-4531	8680 ± 110	9455-10125
Mackay	2	LWBS	AMS 14C	D-AMS 001836	11723 ± 52	13434-13745
Mackay	2	LWBS	AMS 14C	D-AMS 002439	12303 ± 41	14056-14799
Mackay	2	LWBS	AMS 14C	D-AMS 003797	13439 ± 56	15936-16331
Mackay	2	LWBS	AMS 14C	D-AMS 003798	13584 ± 58	16146-16569
Mackay	2	WS	AMS 14C	D-AMS 002440	14131 ± 61	17011-17355
Mackay	2	WS	AMS 14C	D-AMS 001837	13722 ± 49	16340-16777
Mackay	2	BB	AMS 14C	D-AMS 003799	14656 ± 55	17595-18175
Mackay	2	BB	AMS 14C	D-AMS 001838	14706 ± 65	17784-18203
Mackay	2	BWBS	AMS 14C	D-AMS 002440	15309 ± 65	18288-18760
Mackay	2	BWBS	AMS 14C	D-AMS 002441	15342 ± 65	18300-18786
Mackay	2	BWBS	AMS 14C	D-AMS 003800	15871 ± 59	18923-19302
Mackay	2	BWBS	AMS 14C	D-AMS 001839	18232 ± 71	21991-22330

In the second phase of excavation (November 1969), a further nine squares were added towards the centre of the deposit floor. Excavation in most squares was discontinued at the base of Spit 3, around the inferred LSA/MSA contact. Fragments of human remains were found scattered through the upper deposits, something attributed to disturbance of sediment by "dung seekers" (diary entry, 6 December 1969), though one well-preserved burial was recovered from Spit 1 and subsequently dated to 3540 ± 60 BP (Pta-1642) (3593–3971 cal yr BP) (Thackeray, 1977). (All radiocarbon ages are calibrated to SHCal20, following Hogg et al. (2020))

There are two other radiocarbon assays from the upper strata at KFR1—— 5570 ± 70 BP (Pta-2476) (6195-6488 cal yr BP) and 8680 ± 110 BP (Pta-4531) (9455–10125 cal yr BP) (Table 1)—both reported by Nackerdien (1989). The former age comes from the unit 'Horizons above Spit 1' (HAS1), the term given to all surface deposits, typically those comprising a mix of dung and ash. The latter age comes from near the base of Spit 3, around 300 mm below surface (S. Woodborne, pers. comm., 2019), and thus towards the base of Parkington's LSA excavations. Taken together, the radiocarbon ages suggest that the upper part of Parkington's 'brown clayey soil' formed in the early- to mid-Holocene.

The third phase of excavation (late December 1969) involved removal of four new squares towards the front of the shelter, including the only two (Y & W) taken to bedrock. At the start of spit four in this area, MSA artefacts were encountered and attributed to the Howiesons Poort, though the distribution of these artefacts was noted to slope from west to east across the deposit. A further pertinent observation here is that the pre-Howiesons Poort MSA in these squares appeared to the excavators to be quite different in character to that encountered during the original excavation (squares A–D) along the main datum line:

"The cultural material from spit ⑧ V1256[1] looks more like the H.P. [Howiesons Poort] of last Sept's spit ⑤ than it does like the proper MSA. It has a few QZ [quartzite] flakes and a few patinated flakes and blades and no small implements at all. The MSA of Sept was full of nice triangular QZ flakes and of these we have so far seen very few". Diary entry, 17 December 1969.

As can be noted from Parkington's section drawing (Fig. 2B), spit 8 in this area potentially relates to a sedimentary unit that did not extend across the deposit. The diary ceases at this point, and there is no discussion of the distribution or contents of the underlying pale brown unit.

Volman undertook analysis of the MSA material from spits 5–9, assigning spits 5 and 6 largely to the Howiesons Poort (though mixed with overlying LSA and underlying MSA artefacts), and spits 7–9 to unit MSA 2b in his southern African MSA synthesis. The sample from spits 7–9 was assigned to MSA 2b rather than MSA 2a not because of its stratigraphic context but because of its technological composition, including high rates of retouch, the presence of unifacial points, cores with intersecting ridges, and an absence of denticulates (Volman, 1981: 253).

An important note concerning Volman's culture-historic assignments is that at the time the validity of the Still Bay as an independent MSA unit was in question (Sampson, 1974). One consequence was that bifacial point-bearing deposits were often assigned to MSA 2b (Volman, 1981). In fact, KFR1 is the only MSA 2b sample that Volman analysed from which bifacial points were considered to be absent (Volman, 1981: 253). Given the Still Bay assemblage dating 72 ± 4 to 80 ± 5 ka 2 km away at Hollow Rock Shelter (Högberg, 2014, Högberg and Larsson, 2011), this implies that KFR1 was rarely occupied between the Howiesons Poort and the MSA 2b. Intriguingly, however, in Parkington's excavation diary entry for 15 December 1969 he notes that "Cedric [Poggenpoel] has excavated a bifacial 'laurel leaf' point broken at both ends from squares X/Y". This occurred as Poggenpoel was excavating below the level at which bones occurred—and thus within the MSA. Whether and why this artefact was not analysed by Volman is unknown, but it potentially implies the existence of an ephemeral Still Bay at KFR1, aligning it with Volman's other MSA 2b assemblages.

Renewed Work 2011–2012

KFR1 was re-excavated over five 1-month-long seasons in 2011 and 2012. Two separate trenches were excavated at the site. Trench 1 was located towards the front of the shelter immediately south of Parkington's deep sounding (south of the AVW line), and Trench 2 was added later towards the rear of the site away from previously excavated areas (Fig. 2A). The results of the Trench 2 excavations—which relate almost wholly to the late Pleistocene LSA occupation of the site—are published elsewhere (Low, 2019, Mackay et al., 2019).

---

[1] 'V' references the square, and the numbers afterwards reference the subsquares within it. Parkington subdivided each four foot square into 16 one foot subsquares.
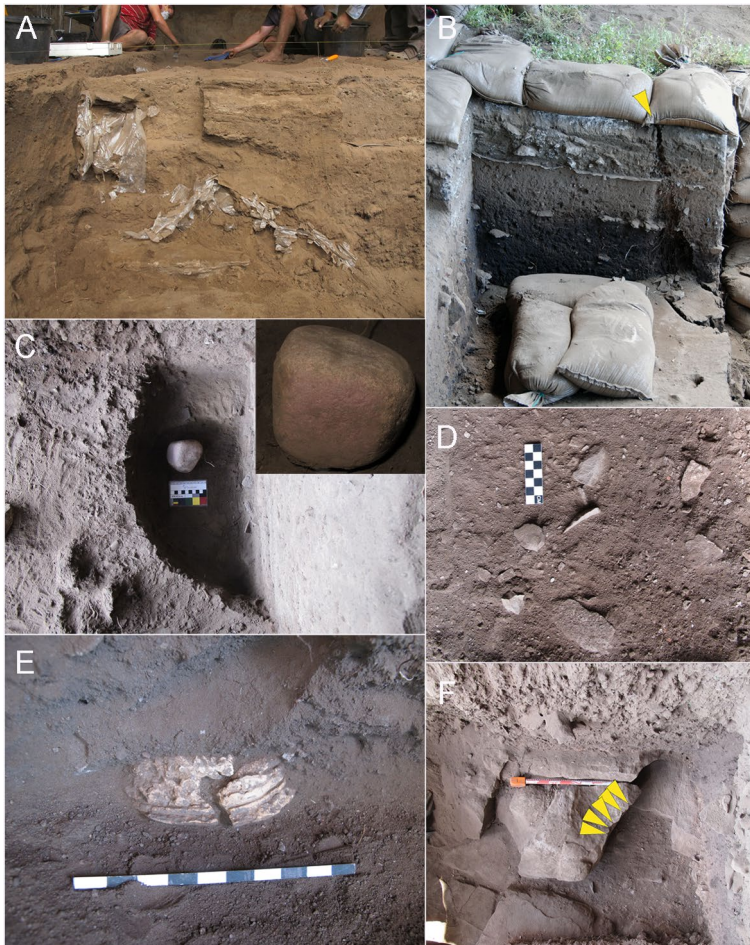
Fig. 4 (**A**) Remains of plastic lining from Parkington's 1969 excavations. (**B**) Cut in the west section [indicated by yellow arrow] as a result of water pooling behind sandbags. (**C**) Ochred and pitted grindstone in the base of the Pit. (**D**) Concentration of artefacts in PBS (scale in cm). (**E**) Trilobite fossil in situ within BSS (scale in cm). Panel **F**: flaked roof fall near base of excavation (scale in 10 cm). Flaking initiations indicated by yellow arrows

It was possible to re-create Parkington's original excavation area by the preservation of his grid marks on the shelter walls, in combination with features such as surface rocks. Plastic sheeting laid at the base of the old excavation was encountered ~200 mm below surface, and again lining the main section in the deep sounding (Fig. 4A). The backfill was removed from the deep sounding squares A, B, V, W, X, and Y, and from the upper (backfill of spits 1–3) deposits in squares E, F, and G. The base of the old excavation in squares A, V, B, and X, which had not been taken to bedrock, was not lined with plastic. This contact thus required extensive cleaning before the residual deposits in this area could be removed. In total, five new 1-m squares were opened in

Trench 1, labelled 1, 2, 3, 4, and 6 (Fig. 3B). Squares 1, 2, and 6 mark a southward extension of Parkington's deep sounding, and corresponding to his squares E, F, and G. Our squares 3 and 4 contain the residual material not excavated by Parkington at the base of A and V. Square 5 exists conceptually but contained only a very small amount of residual deposit above bedrock which was incorporated into Square 4.

Once the old AVW profile was cleaned, the stratigraphy was mapped. As Parkington had previously noted, visible stratigraphy in Trench 1 was limited, and available markers suggested a mix of flat and sloping surfaces with sometimes undulating contacts. Some of the differentiation in sediment colour was a product of variable moisture, which was more prominent to the west side of the section. The reason for this became apparent between Seasons I and II when a leak in the shelter roof on the west side led to surface pooling of water and some erosion of the west section and the north western edge of Square 6 (Fig. 4B).

In total, we mapped five stratigraphic units in the old section before commencing excavation (Fig. 5A). A sixth stratigraphic unit was later differentiated during excavation (Fig. 5B), corresponding to a well-defined pit in the south east corner of the excavation. Unlike Parkington we elected not to excavate following the surface slope of the deposit reasoning that any applied slope would be arbitrary given the visible variation and no more or less likely to avoid cross-cutting. We thus excavated following stratigraphic breaks but proceeding between stratigraphic units in horizontal excavation units not exceeding 30 mm (in other words, excavated in 30 mm spits when stratigraphic units exceeded 30 mm). All finds over 20 mm were plotted with exceptions made for beads, teeth, marine shell, retouched flakes, and cores, to which no size cutoff was applied. On completion of excavation we mapped the new section, allowing us to create bounding boxes for the different stratigraphic units. These also allowed us to reassign individual plotted artefacts to stratigraphic units where strata were cross-cut.

In total we plotted approximately 8000 finds in Trench 1, with the deepest deposits (1.96 m below surface) occurring in Square 2 and the shallowest in Square 6 (1.18 m). While the morphology of the basal deposits maintains the west to east slope noted by Parkington, it is unclear whether our excavations terminated on bedrock or roof-fall. The fragmented nature of the basal rock suggests roof-fall, as does a 0.4-m-deep localised sediment trap between rocks at the base of Square 2 (Fig. 3B).

After the excavation, we undertook geophysical work across the surface to better understand the basal morphology and its influence on the observed structure of the deposits. We present the results of all analyses in the subsequent sections.

Stratigraphic Sequence

Six stratigraphic units are differentiated in Trench 1 at KFR1 (Fig. 5). All, except the pit, slope down to the north-east, though in all cases the slope is steeper than that of the current deposit surface, partly explaining persistent cross-cutting in Parkington's sample.

The youngest unit we identified is referred to as PIT1, which is a vertical shaft 0.8 m deep and ovate in plan. The top of the pit would have been visible at the base
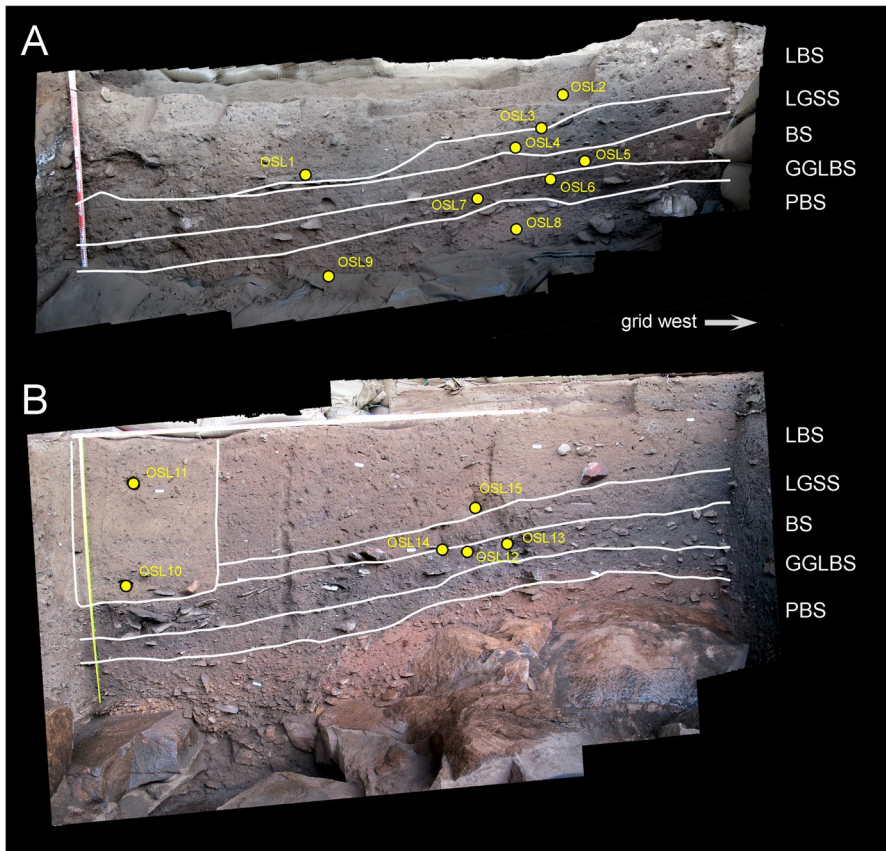
Fig. 5 (**A**) Trench 1 south section and OSL sampling locations prior to commencement of 2011 excavations. (**B**) Trench 1 south section and OSL sampling locations after completion of excavation

of Parkington's squares E, H, T, and U but not in the AVW profile line, as the pit extends only 0.28 m north into square 2. No human remains were encountered in PIT1 though an ochre-covered grindstone appears to have been placed in the base of the pit (Fig. 4C), along with a large quartzite scraper.

The second youngest unit is Light Brown Sand (LBS). This is the only unit to contain significant quantities of organic material, mainly bone, but also some ostrich eggshell and marine shell. There was no apparent substructure to LBS despite a maximum depth of 0.77 m. The base of the unit is defined by the discontinuous black crust; where this is absent the contact to the underlying unit was somewhat ambiguous. All of Parkington's Spits 1–4 fall within LBS, as does part of Spit 5 and potentially Spit 6.

Below LBS is the unit referred to as Light Grey Silty Sand (LGSS). LGSS thins out to the northeast and is truncated by PIT1 in the southeast corner of the excavation. Components of Parkington's Spits 5 and 6 cross-cut LGSS. The same is largely

true of the underlying unit Brown Sand (BS) which intersects the base of PIT1 but extends beyond it into the east section. This unit was cross-cut by Spits 6 and 7.

Below BS and following largely the same slope is the unit Gritty Grey Light Brown Sand (GGLBS), though the base of this unit has a somewhat irregular topography possibly reflecting the morphology of the bedrock which closely underlies it towards the western end. GGLBS seems to be contained almost entirely within Parkington's Spit 7, though the eastern extent of this spit is unclear.

The final unit we identified is Pale Brown Sand (PBS) which incorporates the sediments noted by Parkington as 'Dark brown soil with sandstone grit' and 'Very pale brown soil with small chips of bedrock'—and thus Spits 8 and 9. PBS is quite variable in colour, though colour variance often cross-cuts depositional features such as dip of flat rocks, and appears to track the morphology of the underlying bedrock. We thus surmise that the colour variation is post-depositional and may relate to water seepage across bedrock. While PBS is fairly shallow at the eastern end (~0.2 m), it continues to a depth of 0.67 m at the western end, largely due to the previously noted 0.4 m cavity between rocks at the base of Square 2.

Sediments

Analyses were undertaken on sediment samples recovered during excavation, and from two vertical sample columns taken from the south section after completion of excavation. We were interested to explore a range of variables, including changes in sediment supply, composition, and pH, the last to better understand the causes of poor organic preservation in the MSA contexts noted by Parkington.

We analysed the archaeological deposits from column sequences in Squares 6 and 2 in the final south section of Trench 1 to measure organic and carbonate proportions (using Loss on Ignition), Magnetic Susceptibility (MS), and pH (Table 2). Both organic and carbonate proportions generally decline through the sequence though values from the Square 2 column are typically higher than those from Square 6 (for location reference, see Fig. 3B). This distinction is most notable in the carbonate fraction and may reflect leaching from increased water seepage on the western side of the trench where Square 6 occurs (Goldberg and Macphail, 2006).

MS, which can indicate difference sediment sources or episodes of sediment transformation due to weathering or anthropogenic burning (Dalan and Banerjee, 1998), reveals similar sequential trends but reversed horizontal trends to organic and carbonate proportions. MS values decrease down-sequence in both columns, though values in the Square 6 column are higher than those in the Square 2 column. The MS values for both low- and high-frequency suggest a major decrease from LBS and LGSS to BS, with low values persisting thereafter. Whether this reflects a change in occupational intensity or sediment mineralogy is unclear. Elevated MS values remerge in the deepest PBS samples from the Square 2 column, which correspond to the depression at the base of that square.

The most appreciable difference between the two column sequences, however, is in pH. The samples from Square 2 are either alkali (>7.0) or neutral (7.0) with the

Table 2 Loss on Ignition (LOI), magnetic susceptibility (MS) at High Frequency (HF) and Low Frequency (LF), and pH for column samples from Squares 2 and 6. Samples increase in depth by sample number in increments of 50 mm. 'PBS (Lower)' refers to that part of the section within the depression at the base of Square 2

Stratum	Column sample #	LOI % organic		LOI % carbonate		MS LF mass		MS HF mass		pH	
		Sq6	Sq2	Sq6	Sq2	Sq6	Sq2	Sq6	Sq2	Sq6	Sq2
LBS	1	4.23	4.62	1.58	3.27	220.35	212.83	201.83	197.6	6.5	8.9
	2	3.83	4.81	1.34	2.34	300.49	187.2	286.06	173.12	6.57	8.03
	3	3.15	5.32	0.89	1.89	210.33	184.2	195.37	169.9	5.5	8.63
	4		5.42		1.38		158.42		144.34		8.03
	5		4.7		1.12		99.6		91.34		8.27
LGSS	6	3.44	5.43	0.76	1.17	148.58	180.57	138.43	174.49	5.33	7.7
BS	7	3.52	4.86	0.69	1.27	155.91	93.38	143.49	86.01	5.23	7.33
	8	2.18	3.16	0.48	0.65	120.66	80.73	112.79	74.38	5.07	7.53
GGLBS	9	1.45	2.31	0.7	0.47	103.87	84.83	94.39	81.19	5.5	6.53
PBS	10	1.1	1.68	0.63	0.63	101	102	92.03	92.99	4.9	7.2
	11		1.81		0.52		77.23		70.89		6.7
	12		1.88		0.66		91.56		107.52		7.07
PBS (lower)	13		2.28		0.66		106.24		97.28		7.17
	14		2.37		0.67		155.57		149.59		6.47
	15		2.33		0.83		113.11		102.64		5.77

exception of the lowermost samples that have pH values of 5.7–7.1. The Square 6 samples, however, are weakly acidic towards the top of the deposit, but acidic to strongly acidic below (<7.0), revealing poor preservation conditions in these deposits. Acidity trends across the deposit are likely linked to the generally greater moisture at depth and in Square 6 relative to Square 2 (Reidsma et al., 2021).

Geophysics

Two geophysical techniques were employed to map bedrock morphology at KFR1: ground-penetrating radar (GPR; summarised for archaeological applications by Conyers (2013)) and electrical resistivity tomography (ERT; summarised for pedological applications by Samouëlian et al. (2005) and more generally by Loke et al. (2013)). The specific methods and equipment used are described in SOM. Both techniques were applied post-excavation after the site had been backfilled with sandbags and sterile sand.

At KFR1, both the GPR and ERT data reveal a complex basal morphology that varies between 0.25 m and 1.9 m below the deposit surface (Fig. 6). The thickest unexcavated accumulations of sediment in the shelter occur immediately south of Trench 1, approximately as deep as the maximum depth (1.96 m) obtained in the cavity at the base of Square 2 (Fig. 4B). The roughly SW-NE alignment of thicker deposits may suggest a structural control on the basal geomorphology.
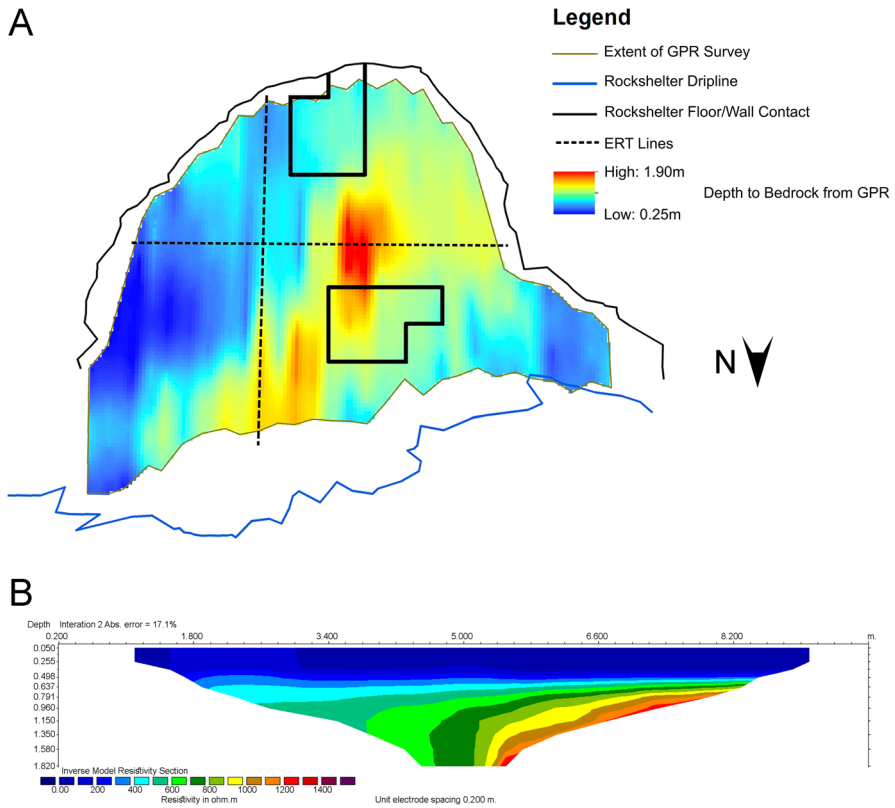
Fig. 6 (**A**) Interpretation of deposit depth across KFR 1 based on the GPR survey, with 2011–2012 excavation trenches shown as black outlines and ERT lines indicated by dashed lines. (**B**) Results of north to south ERT line

The basal surface is recognisable in GPR profiles as a high amplitude reflector which is somewhat discontinuous, although this feature is very difficult to see where backfilled excavation is present. Air wave reflections from the roof are recognisable in the profile, however have an apparent depth which is deeper than the bedrock surface in all cases so do not confuse interpretation. Unconsolidated unexcavated sediment within the rockshelter is relatively homogenous and shows a very low amplitude response. In contrast, areas that have been excavated and backfilled show a complex, high amplitude response, probably reflecting sandbags used in the backfill.

ERT data collection was made difficult by high contact resistance (up to ~5000 Ohm) that could not be overcome by watering the electrodes with salty water. As a result, RMS (root mean square) error results for the inversions were high, particularly for the relatively low current Dipole-Dipole array (>100%), so we choose to use Wenner array results exclusively for data interpretation. While this decision led to more robust inversions it compromised both data density and depth of investigation (Dahlin and Zhou, 2004).

The interpretation of the basal surface using ERT was relatively challenging, with no discrete boundary in resistivity values observable in the data. Despite the lack of clear boundaries, unconsolidated sediment values are less resistive (~20 to 800 ohm m) with an obvious low resistivity layer (<200 ohm m) present in the top 0.5m. This layer may be lithological but more likely reflects the impact of extensive watering of the electrodes. Bedrock values are in the range of 600 to 1400 ohm m. The lack of an obvious discrete contrast between bedrock and unconsolidated sediments probably reflects the extreme low moisture content of the sediments and results in some disparities between the interpretation of depth to bedrock between ERT and GPR.

Chronological Sequence

We used single-grain OSL dating of sediments to obtain burial ages (Huntley et al., 1985; Aitken, 1998; Duller, 2004; Wintle, 2014; Roberts et al., 2015) for fifteen samples collected from each of the stratigraphic units of Trench 1 (Fig. 5). Samples OSL1–9 were collected from the original south section at the start of Season I (Fig. 5A), and OSL10–15 from the new south section at the end of Season II (Fig. 5B). The two sampled sections are 1 m apart. All samples, except OSL1, were collected by hammering PVC tubes (~5 cm in diameter, ~15 cm long) into cleaned section walls, and were sealed in light-proof black plastic. OSL1 was collected from the black crust as a small intact sediment block sample that was also sealed in black plastic. A separate sediment sample was collected at each sample location for laboratory measurements of present-day sample moisture content and environmental radioactivity.

Environmental radiation dose rates were calculated as the sum of the beta, gamma, and cosmic-ray dose rates. Sand-sized quartz grains of 180–212 μm diameter were isolated for OSL dating and purified using standard procedures (e.g., Wintle, 1997). Single grains of quartz were measured using the single aliquot regenerative-dose (SAR) procedure and experimental apparatus described elsewhere (Bøtter-Jensen et al., 2003; Murray & Wintle, 2000). All single-grain data were analysed using two different approaches: the conventional approach (e.g., Jacobs et al., 2008; Approach A) and the L_nT_n method (Li et al., 2016, 2017, 2020; Jacobs et al., 2017; Hu et al., 2019, 2020; Fu et al., 2020; Zhang et al., 2020; Approach B). The latter method is useful when a sample contains a significant proportion of grains with 'saturated' natural signals that are rejected because a finite equivalent dose (D_e) value cannot be obtained. This may truncate the D_e distribution of the sample and lead to underestimation of the final D_e value, and therefore the age (e.g., Duller, 2012; Gliganic et al., 2012; Thomsen et al., 2016; Guo et al., 2017; Li et al., 2017). The D_e, dose rate, and age estimates are summarised in Table 3, together with information about the analytical methods used. Uncertainties are given at 1σ (the standard error on the mean). Further detail on the methods used for D_e determination are provided in SI.

There is not a distinct trend in environmental dose rate with depth; values range from 1.33 ± 0.05 Gy/ka (OSL13) to 1.75 ± 0.06 Gy/ka (OSL2) (Table 3). Four

Table 3 Dose rate data, equivalent dose (D_e) and overdispersion (OD) values, and OSL ages for samples collected from KFR1

Sample	DBS (cm)	External dose rate (Gy/ka)		Total dose rate (Gy/ka)[d]	No. of grains[e]	Analytical approach[f]	OD (%)[g]	D_e (Gy)	Age model[h]	Age (ka)[i]
		Beta[b]	Gamma[c]							
PIT1										
OSL10	17	0.777 ± 0.035	0.672 ± 0.030*	1.528 ± 0.048	101/500	A	40 ± 3	13.0 ± 0.6	CAM	**8.5 ± 0.5**
OSL11	58	0.754 ± 0.034	0.701 ± 0.032*	1.533 ± 0.048	220/1000	A	42 ± 2	12.9 ± 0.4	CAM	**8.4 ± 0.4**
Light Brown Sand										
OSL2	21	0.948 ± 0.042	0.723 ± 0.041	1.749 ± 0.060	269/1000	A	65 ± 3 (42)	20.0 ± 1.5	FMM2 (79%)	**11.4 ± 1.0**
								64.4 ± 10.1	FMM3 (15%)	36.8 ± 5.9
OSL15	37	0.764 ± 0.035	0.692 ± 0.031*	1.534 ± 0.048	186/800	A	89 ± 5 (29)	11.8 ± 1.3	FMM1 (19%)	7.7 ± 0.9
								30.5 ± 1.9	FMM2 (44%)	19.9 ± 1.4
								107.9 ± 5.6	FMM3 (37%)	70.3 ± 4.5
Boundary between Light Grey Silty Sand and Light Brown Sand										
OSL3	31	0.800 ± 0.037	0.593 ± 0.039	1.472 ± 0.054	287/1000	A	75 ± 3 (34)	23.0 ± 1.4	FMM1 (50%)	15.7 ± 1.2
								75.6 ± 3.8	FMM2 (45%)	51.4 ± 3.4
OSL1	49	0.936 ± 0.042	0.593 ± 0.031	1.608 ± 0.053	150/1000	B	27 ± 7 (18)	91.7 ± 3.8	CAM+nMAD	**57.0 ± 3.2**
Light Grey Silty Sand										
OSL4	43	0.811 ± 0.037	0.672 ± 0.050	1.561 ± 0.063	376/1000	A	77 ± 3 (30)	12.5 ± 1.4	FMM1 (13%)	8.0 ± 1.0
								28.2 ± 1.8	FMM2 (38%)	18.1 ± 1.4
								85.9 ± 3.3	FMM3 (49%)	55.0 ± 3.2
Brown Sand										
OSL5	50	0.729 ± 0.034	0.595 ± 0.042	1.402 ± 0.055	294/900	A	46 ± 3 (22)	29.9 ± 1.7	FMM1 (13%)	21.3 ± 1.5
								95.2 ± 2.1	FMM2 (87%)	**67.9 ± 3.4**
OSL14	56	0.732 ± 0.034	0.665 ± 0.050	1.475 ± 0.061	167/1000	A	77 ± 5 (36)	23.3 ± 1.7	FMM1 (28%)	15.8 ± 1.4
								103.7 ± 4.8	FMM2 (72%)	**70.3 ± 4.6**
OSL12	62	0.815 ± 0.037	0.644 ± 0.029*	1.537 ± 0.048	200/1000	A	62 ± 4 (23)	25.4 ± 1.3	FMM1 (18%)	16.5 ± 1.0
								105.8 ± 2.6	FMM2 (82%)	**68.8 ± 3.1**
OSL13	64	0.663 ± 0.031	0.589 ± 0.042	1.330 ± 0.054	228/900	B	26 ± 2 (13)	115.9 ± 3.1	CAM+nMAD	**87.1 ± 4.6**
									Mean ± stdev.	
									(excl. OSL13)	*69 ± 1*

Table 3 (continued)

Sample	DBS (cm)	External dose rate (Gy/ka)[a]		Total dose rate (Gy/ka)[d]	No. of grains[e]	Analytical approach[f]	OD (%)[g]	D_e (Gy)	Age model[h]	Age (ka)[i]
		Beta[b]	Gamma[c]							
Gritty Grey Light Brown Sand										
OSL6	57	0.695 ± 0.033	0.566 ± 0.033	1.339 ± 0.048	144/1000	B	41 ± 5 (18)	121.2 ± 4.2	CAM+nMAD	**90.5 ± 4.9**
OSL7	62	0.727 ± 0.034	0.723 ± 0.040	1.528 ± 0.053	197/900	B	48 ± 6 (16)	28.0 ± 7.0	FMM1 (22%)	18.3 ± 4.6
								122.6 ± 23.2	FMM2 (73%)	**80.2 ± 15.5**
									Mean ± stdev.	*85 ± 7*
Pale Brown Sand										
OSL8	78	0.651 ± 0.031	0.659 ± 0.038	1.388 ± 0.051	172/1000	B	24 ± 3 (14)	229.9 ± 15.9	CAM+nMAD	**165.6 ± 13.4**
OSL9	91	0.685 ± 0.032	0.698 ± 0.045	1.461 ± 0.056	148/1300	B	22 ± 2 (14)	213.8 ± 20.9	CAM+nMAD	**146.3 ± 15.6**
									Mean ± stdev.	*156 ± 14*

[a] Includes a cosmic-ray dose rate of 0.045 ± 0.007 Gy/ka. All beta and gamma dose rates were adjusted for an assumed long-term water content of 5 ± 2.5%; measured water contents ranged from 2.4 to 10.4% (mean = 5.3%)

[b] Beta dose rates were calculated using a Risø GM-25-5 multi-counter system, measuring dried, homogenised powdered sediment samples

[c] Gamma dose rates were calculated using elemental concentrations of U and Th (estimated using thick source alpha counting) and K (estimated using inductively coupled plasma optical emission spectroscopy). Gamma dose rates were directly measured, using a field gamma spectrometer, for samples indicated with an asterisk

[d] Includes an assumed internal quartz alpha dose rate of 0.033 ± 0.008 Gy/ka

[e] The number of grains used for final D_e determination/the total number of grains measured

[f] D_e determination for most grains was done following a conventional approach (Approach A) where the sensitivity-corrected natural signal (L_n/T_n) is projected onto the dose response curve for each grain to obtain a distribution of D_e values, or the '$L_n T_n$' method of Li et al. (20162020202020) (Approach B) where the distribution of re-normalised L_n/T_n ratios are analysed and combined, and the combined value projected onto a standardised dose response curve (SGC) to obtain a single D_e value. All data analyses for D_e determination were undertaken in *R* (R Core Team,) using packages *numOSL* (Peng et al., 2013; Peng & Li, 2017) and *Luminescence* (Kreutzer et al., 2012; Kreutzer et al., 2021)

[g] OD values calculated using the CAM. Values in brackets represent the OD used for either the FMM or calculated after rejection of outliers using nMAD

[h] FMM components comprising less than 10% of the accepted grains are not listed

[i] Values highlighted in bold represent the age for the main D_e component, when clearly distinguishable (i.e., representing >60% of the accepted grains)
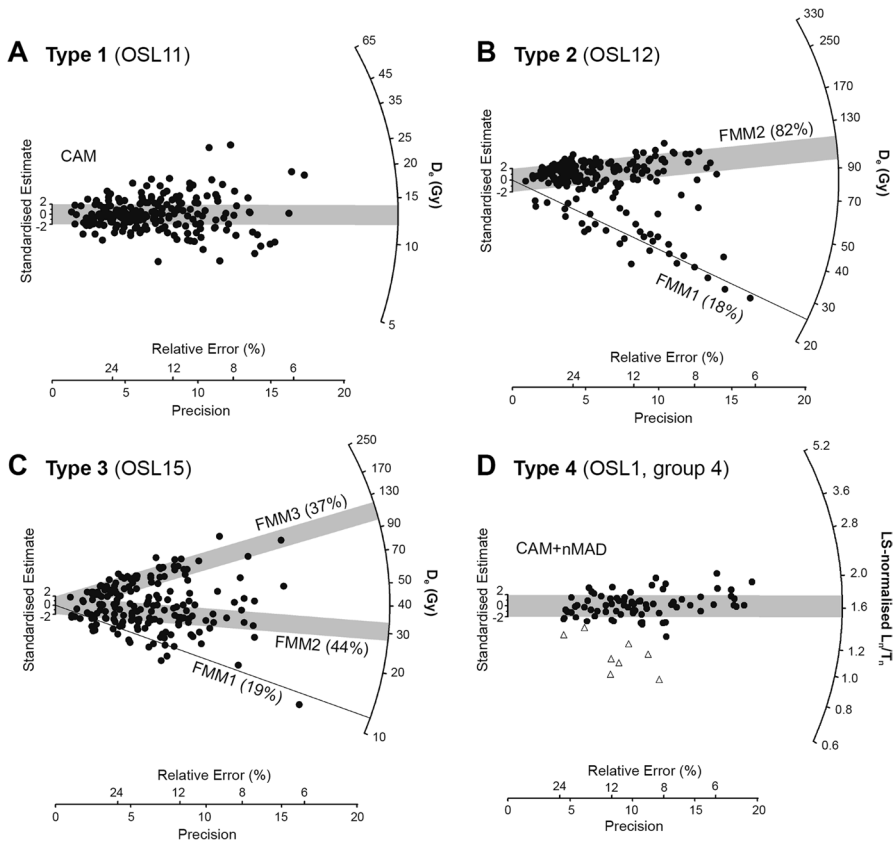
Fig. 7 (**A–D**) Representative radial plots of the dose distributions obtained from single-grains of quartz at KFR1. The grey bands or thin lines projected onto the radial axes are each centred on a value used to calculate D_e. Open triangles indicate rejected outliers

different types of dose distributions were observed. Radial plots for a representative sample from each type are shown in Fig. 7 and the rest in Figure S3 and S5. The first distribution type represents samples with simple D_e distributions indicative of grains that were well-bleached and that remained relatively undisturbed since burial (OSL10 and OSL11); the central age model (CAM) of Galbraith et al. (1999) was used to combine all D_e values for age determination (Fig. 7A, Table 3). The second distribution type represents samples that consist of two or three discrete D_e components, one of which is dominant (>60% of grains, Fig. 7B, OSL2, 5, 12, 14). The finite mixture model (FMM) together with maximum log likelihood and Bayesian information criterion tests were used to determine the number of components, their overdispersion value, and a weighted mean D_e determined for each component (e.g., Galbraith & Roberts, 2012; Table 3). For such samples, the D_e and resulting age of the major component were thought to represent the depositional age of the stratigraphic unit and grains associated with the minor component are interpreted

as intrusive. The third distribution type shows a more complex mixture of grains (OSL3, 4, 15). Different dose components are still discrete and application of the FMM suitable, but there is no dominant or major component (Fig. 7C; Table 3). The stratigraphic integrity of such samples is compromised. The fourth distribution type is for samples that contained a significant number of grains with D_e values that were in dose saturation and for which the L_nT_n method of analysis was used instead; this included six samples (OSL1, 6, 7, 8, 9, 13; Table 3). An example of the distribution of re-normalised L_n/T_n ratios (rather than D_e values) for one group of one sample is shown in Fig. 7D. The re-normalised L_n/T_n distributions for all six samples are like those of Type 2. With the exception of OSL7, intrusive grains were identified as statistical outliers using the normalised median absolute deviation (nMAD) test (Powell et al., 2002; Rousseeuw et al., 2006), rather than the FMM. All accepted grains were then combined using the CAM. For OSL7, which contained more significant mixing, the FMM was applied on the re-normalised L_n/T_n ratios to obtain the D_e of each component, in each group. The same dose components were identified in each non-saturated group, and so the weighted mean D_e of each component was used for age determination (Table 3).

The discrete dose components and resulting age estimates (Table 3) suggest that sediment deposition was discontinuous over a period of time that started 166 ± 13 ka (OSL8) during MIS 6 and finished 11 ± 1 ka (OSL2) at the end of the Pleistocene. PBS, the lowest stratigraphic unit, was deposited 156 ± 14 ka (mean and standard deviation). This was followed by a significant hiatus in sediment deposition that lasted for ~70 ka, after which unit GGLBS was deposited 85 ± 7 ka (mean and standard deviation). Paired samples from both units gave OSL ages that are statistically consistent. A single sample from the overlying unit BS (OSL13) has a D_e value and age that is consistent with those from GGLBS, but significantly different from other samples from the same unit. The remaining three samples from BS (OSL5, 12, and 14) gave statistically consistent ages with a mean age and standard deviation of 69 ± 1 ka. LGSS overlies BS and is in turn overlain by a discontinuous black crust. OSL1 was collected from an intact portion of the crust in the central west portion of the trench (Fig. 5A) and gave an age of 57 ± 3 ka. This is also a minimum age for the underlying LGSS. Only one sample (OSL4) was collected from LGSS, but its D_e distribution displayed significant evidence for post-depositional mixing, with sediments last exposed to sunlight at 8 ± 1 ka (13%), 18 ± 1 ka (38%), and 55 ± 3 ka (49%). The latter age is consistent with the age for the overlying black crust, and the distribution of ages similar to that obtained for OSL3 (Table 3). Two samples (OSL2 and OSL15) were dated from the uppermost unit LBS. OSL2, collected from the middle of the unit, is dominated by a component of grains that were deposited 11 ± 1 ka. OSL15, collected from the boundary between LGSS and LBS, is much more dispersed. The final event dated is the PIT1 feature; two samples from the top and bottom of the feature gave almost identical ages of ~8.5 ka.

Despite the abundant evidence for varying degrees of post-depositional mixing at KFR1, single-grain OSL dating has afforded the ability to observe and isolate legacies of disturbances to the sedimentary deposits. This enabled calculation of burial ages for the archaeological assemblages within much of the site, and attests

to the general stratigraphic integrity for the PBS, GGBS, and BS deposits. Interestingly, however, even within the mixed LBS sediment sampled by OSL15, populations of grains last exposed to sunlight 70 ± 5 ka (37%), 20 ± 1 ka (44%), and 8 ± 1 ka (19%) were able to be identified, which are consistent with the Howiesons Poort, MIS 2, and Holocene stone artefacts noted around the sample location during extraction. Two pulses of post-depositional disturbance can be identified at KH1, the first during MIS 2 (OSL3, 4, 5, 7, 12, 13, 14, 15) and the second ~8 ka (OSL4, 10, 11, 15) which includes PIT1 formation.

Palaeoecology

Palaeoecological data at KFR1 derive exclusively from phytoliths extracted from sediments samples taken in layers BS, GGLBS, and PBS, and thus covering MIS 4 (*n*=3), late MIS 5 (*n*=3), and MIS 6 (*n*=3); few wood charcoal and no other organics were preserved in these deposits (see below). The signal from phytoliths is mediated by human choices about which plant items to transport to site, and consequently does not strictly reflect the palaeoecology of the site and its surrounds (Esteban et al., 2018). However given the placement of KFR1 at the modern boundary of the Fynbos and Succulent Karoo biomes we are interested to explore whether there were any indicators of turnover at the community level across the two glacial and one inter-glacial stages represented.

Phytolith preparation followed established methods (Piperno, 2006). Phytoliths were extracted from nine samples of approximately 5 g of bulk sediment fine fraction. Samples were deflocculated overnight in a 0.05% $NaPO_3$ solution, then sieved through a 125 μm mesh and dried. ~1 g samples were sub-sampled from the <125 μm fraction. Samples were treated with 10% HCl in 10 ml aliquots to remove carbonates. Clays were deflocculated by suspending samples in 0.05% $NaPO_3$ solution, followed by decantation according to Stokes Law, repeated three times. Organic matter was digested with a quick rinse of samples in 10% KOH solution, followed by another three rounds of clay deflocculation. Samples were neutralised and rinsed with distilled water three times between all steps. Phytoliths were extracted by flotation using sodium polytungstate at a density of 2.3 g/cm^3. Phytolith extracts were rinsed, dried on a hotplate, and mounted onto microscope slides using Entellan.

Identification and counting of phytoliths were conducted at 400× magnification using an Olympus Bx51 light microscope with polarising light. Classification follows the ICPN 2.0 (Neumann et al., 2019). Phytoliths were counted to 300 per sample, and the percentage of slide counted estimated. Indicators of taphonomic damage, such as dissolution, etching, and breakage, were also recorded. Results are presented in concentration per gram of sediment (pgs), estimated from the raw phytolith count, percentage of slide examined, and the ~1 g weight. Two key indicator indices were calculated: C^4 to C^3 grasses, and the Fy index. The C^4/C^3 ratio was calculated by dividing the sum of C^4-diagnostic grasses by the sum of C^3-diagnostic grasses and multiplying by 100, to clearly represent C^4 grasses in the C^3 dominated winter rainfall zone of southern Africa. The Fy index (a measure of the relative abundance of fynbos vegetation) from

Esteban et al. (2017) was calculated by diving the sum of Restionaceae and spheroidal (woody) phytoliths by the sum of short cell phytoliths. Average index values for each unit were calculated using the average phytolith counts across the unit for each morphotype.

Phytoliths were recovered from all nine samples analysed; however, two samples had very low concentration values of 3409 and 3640 phytoliths per gram of sediment (pgs); the other seven samples ranged from 17,731 to 56,327 pgs. These two samples also displayed anomalous C^4/C^3 index values (13.6 and 113.6), and therefore were excluded from further analysis due to possible taphonomic influences, particularly on the short cells. Otherwise the assemblages feature moderate signs of dissolution and minor breakage, with the average proportion of damaged phytoliths increasing from unit PBS through to unit BS (Table 4). Restionaceae phytoliths are relatively abundant across all samples, greatly outnumbering short cell (Poaceae) morphotypes, and consisting of >20% of the total assemblage across all seven samples. Non-graminoid phytoliths are always less abundant than short cells, but found at moderate concentrations declining on average through time; woody phytoliths, specifically, consist of almost 10% of the total assemblage in unit PBS, but make up <4% in unit BS. Short cell phytoliths are almost exclusively dominated by C^3 morphotypes across units PBS and GGLBS, with C^4/C^3 ratios between 20.0 and 42.9; however, there is a moderate rise in the C^4/C^3 ratio in unit BS sample A to 71.4. The Fy index slightly rises over time from 1.9 (sample C unit GGLBS) and 2 (sample C unit PBS), to a maximum of 4.5 (sample A unit GGLBS), and a value of 3.7 in unit BS sample A.

The high incidence of Restionaceae, with moderate non-graminoid (woody and shrubby) vegetation across all samples indicates the continuing dominance of fynbos vegetation at this site over time. This abundance of Restionaceae, as well as a significant incidence of C^3 grasses, is consistent with the region's winter rainfall zone (Cordova, 2013). Unit PBS features slightly higher proportions of Poaceae and woody vegetation than the succeeding units, although the Fy index remains relatively stable across all samples, suggesting some shifts in fynbos vegetation structure since ~150 ka. There is also a moderate rise in the proportion of C^4 grasses in the most recent sample of unit BS, and small declines in Restionaceae and woody vegetation. These changes may suggest a shift in rainfall seasonality and/or drier conditions, although they also reflect conditions similar to those of the Succulent Karoo, where C^4 and Crassulean Acid Metabolism (CAM) vegetation dominates (Scott et al., 2021, Cordova and Scott, 2010, Cordova, 2013).

Cultural Sequence

Description of the cultural sequence at KFR1 derives largely from cataloguing of the piece-plotted fraction of excavated material, though we make some use of data from O'Driscoll's ongoing detailed analysis. The data presented are sufficient to depict the general characteristics and integrity of the assemblages from each stratigraphic unit, but not to make specific statements about behavioural or technological change. The sample from PIT1 is excluded as artefacts in the pit fill were not systematically plotted.

Table 4 Phytolith morphotype classifications and concentrations (per gram of sediment) for sediment samples and units, including indices and proportions for ecologically significant taxonomic groups

Phytolith concentration per gram of sedimenr (pgs)

Unit	BS		GGLBS			PBS	
Sediment samole #	142	154	205	234	296	426	590
	A	B	A	B	C	A	B
Rondel	406	1634	231	1781	1517	517	1955
Crenate	406	109	0	127	690	0	533
Trapezoid	948	1307	693	1908	1793	1263	3731
Cross	0	0	0	0	0	0	0
Polylobate	0	0	0	0	0	115	0
Short saddle	1354	872	231	1781	1104	976	1777
Plateau saddle	0	0	0	0	0	0	0
Round saddle	271	327	58	1145	138	345	1244
Wide bilobate	0	0	0	254	0	57	533
Narrow bilobate	0	0	0	0	0	0	178
Flat bilobate	271	545	0	509	552	115	888
Trapezoidal bilobate	0	545	0	0	552	57	178
Tower	0	218	173	127	414	115	888
Total short cells	**3656**	**5556**	**1386**	**7631**	**6760**	**3560**	**11905**
Discoidal	9479	8389	4332	14881	9243	6488	15637
Reniform	1083	327	173	1526	138	1263	1066
Paddle-shape	1354	1307	924	3943	1380	459	1066
Total restio	**11917**	**10023**	**5429**	**20350**	**10760**	**8211**	**17769**
Other gram	24511	18630	10107	20859	25797	7809	21145
Total gram	40084	34209	16923	48841	43316	19579	50819
Spheroid psilate	1354	1198	462	1272	2207	1263	2665
Spheroid echinate	271	0	347	1526	138	804	2843
Total woody	1625	1198	809	2798	2345	2067	5508
Other non-gram	271	0	0	382	0	0	0
Total non-gram	1896	1198	809	3180	2345	2067	5508
Total phytoliths	**41980**	**35407**	**17732**	**52021**	**45661**	**21646**	**56327**
Fy Index	3.7	2.0	4.5	3.0	1.9	2.9	2.0
C4/C3(x100)	71.4	20.0	23.5	38.1	27.2	42.9	28.3
Poaceae %	8.7	15.7	7.8	14.7	14.8	16.4	21.1
Restio %	28.4	28.3	30.6	39.1	23.6	37.9	31.5
Woody %	3.9	3.4	4.6	5.4	5.1	9.5	9.8

Total values for major phytolith groups are presented in bold

Organic Finds

In the sandstone rock shelters of the Cederberg, preservation of bone and other organic items is typically restricted to the Holocene and early Pleistocene LSA (Mackay et al., 2015, Mackay, 2010, Högberg, 2014). In the rear trench at KFR1,

Table 5 Number of plotted organic finds by stratum. *OES* ostrich eggshell

Stratum	N bone fragments	N OES	N marine shell
LBS	469	17	2
LGSS	16	0	0
BS	8	0	0
GGLBS	2	0	0
PBSS	2	0	0

bone is preserved in the LSA through to ~22 ka but not in the MSA (Mackay et al., 2019). This is also the case in Trench 1, where organic items are essentially restricted to LBS (Table 5). Perhaps more notable is the relationship Parkington observed between the distribution of organic items and the horizon formed by the black crust. Other than four isolated and presumably intrusive bone fragments in GGLBS and PBS, all other organic items either overlie or occur immediately below the crust. The ~45 kyr between deposition of LBS and LGSS presumably explains the disappearance of bone at this stratigraphic transition, which also suggests that assemblage mixing was largely restricted to the contact between these two units, further substantiated by the more extensive mixing shown by single-grain OSL dating. Interestingly, despite the less acidic sediments, preservation of bone is no better in the eastern side of the excavation area than the western side.

Stone Artefacts

The lithic assemblage description provided below concentrates on the results of basic artefact classification in terms of class and raw material (Table 6), and aspects of typology (Tables 7 and 8). Limited supplementary observations are drawn from O'Driscoll's refined analysis of the lower (GGLBS and PBS) samples from Squares 1, 2, and 6, where appropriate (Table 9).

LBS

The LBS sample comprises 899 plotted stone artefacts with recorded attributes. Quartz and hornfels are the most common raw materials, while quartzite and sandstone occur at their lowest proportions in the sequence (albeit that quartzite remains common). Quartz, quartzite, and sandstone can all be acquired in the immediate vicinity of the shelter; however, the nearest source of hornfels is the Doring River, located a minimum straight-line distance of 13 km to the north east. Scrapers and scaled pieces are the major implement types, along with a single 'naturally backed knife'—a distinctive D-shaped scraper made on hornfels acquired from primary sources in the interior Karoo (Orton, 2006). The other scrapers include three end-scrapers and two round scrapers. Core types include bipolar, rotated, and platform

Table 6 Lithics: technological class and rock type by stratum. Counts excludes artefacts for which no technological class or rock type was recorded; totals thus differ slightly from values in the text and Tables 8 and 9

Stratum	Class	*N*	Quartzite	Hornfels	Quartz	Silcrete	Sandstone	Chert	Other
LBS	Flake	645	22.9	42.3	18.3	11.2	1.6	2.8	0.9
	Retouched	60	6.7	43.7	21.7	23.3	0.0	10.0	1.7
	Core	71	11.3	21.1	52.1	8.5	1.6	2.8	0.9
	Fragment	44	31.8	22.7	34.1	6.8	2.3	2.3	0.0
	Heat sh.	37	10.8	73.0	10.8	2.7	0.0	2.7	0.0
	Total	*857*	*20.8*	*40.5*	*21.8*	*11.2*	*1.3*	*3.6*	*0.8*
LGSS	Flake	255	28.2	28.2	11.4	22.7	1.2	4.7	3.5
	Retouched	21	19.0	14.3	9.5	47.6	0.0	4.8	4.8
	Core	23	8.7	21.7	56.5	4.3	0.0	4.3	4.3
	Fragment	10	0.0	10.0	60.0	10.0	10.0	0.0	10.0
	Heat sh.	6	16.7	50.0	0.0	16.7	0.0	0.0	16.7
	Total	*315*	*25.1*	*26.7*	*15.9*	*22.5*	*1.3*	*4.4*	*4.1*
BS	Flake	569	44.8	12.8	8.4	16.0	3.0	2.8	12.1
	Retouched	41	41.5	14.6	2.4	22.0	0.0	7.3	12.2
	Core	34	29.4	8.8	20.6	20.6	2.9	11.8	5.9
	Fragment	29	20.7	17.2	20.7	6.9	6.9	6.9	20.7
	Heat sh.	12	8.3	50.0	0.0	16.7	0.0	0.0	25.0
	Total	*685*	*42.2*	*13.6*	*9.1*	*16.2*	*2.9*	*3.6*	*12.4*
GGLBS	Flake	397	57.7	3.8	5.8	6.0	12.3	0.3	14.1
	Retouched	35	51.4	5.7	11.4	8.6	5.7	2.9	14.3
	Core	17	35.3	5.9	5.9	0.0	29.4	0.0	23.5
	Fragment	50	18.0	0.0	30.0	6.0	12.0	0.0	34.0
	Heat sh.	7	28.6	28.6	0.0	14.3	0.0	0.0	28.6
	Total	*506*	*52.2*	*4.0*	*8.5*	*6.1*	*12.3*	*0.4*	*16.6*
PBS	Flake	2486	46.1	0.4	3.2	1.2	16.7	0.0	2.3
	Retouched	171	74.3	0.0	1.8	1.8	15.8	0.0	6.4
	Core	88	29.5	0.0	5.7	1.1	59.1	1.1	3.4
	Fragment	195	23.6	1.0	11.8	0.0	55.9	0.0	7.7
	Heat sh.	13	15.4	23.1	0.0	7.7	7.7	0.0	46.2
	Total	*2953*	*45.6*	*0.5*	*3.8*	*1.2*	*45.7*	*0.1*	*3.1*

Table 7 Lithics: main implement types. The single naturally backed knife in LBS is included in the scraper column

Stratum	Backed	Burin	Denticulate	Notched	Scaled piece	Unifacial point	Scraper
LBS	1	0	2	2	8	1	24
LGSS	1	0	0	1	1	0	3
BS	5 (2)	4	3	4	3	3 (1)	1
GGLBS	0	2	8	7	0	1	1
PBS	0 (1)	2	66	24	0	3	0
Total	7 (3)	8	79	38	12	8 (1)	28

Table 8 Lithics: main core types, following Mackay et al. (2015). Cores assigned 'no type' are those that did not conform to any of the simplified classes used below, including cores with three or fewer flake scars and prepared cores that could not be classed as Levallois

Stratum	Bipolar	Discoidal	Levallois	Single platform	Rotated (multi platform)	No type
LBS	15	0	6	2	8	43
LGSS	11	1	3	1	0	10
BS	6	4	0	9	5	10
GGLBS	0	5	2	3	0	7
PBS	1	6	3	32	10	36
Total	33	16	14	47	23	106

Table 9 Lithics: frequency of blades and convergent flakes, and as a proportion of complete flakes. GGLBS and PBS data only

Stratum	Blades		Convergent flakes		Complete flakes
	N	$\%$	N	$\%$	N
GGLBS	24	16.4	43	29.5	146
PBS	104	9.8	240	22.6	1063

cores, with bipolar the most common. A single silcrete platform core was described in the excavation notes as being of likely Robberg association. Overall, the characteristics of the LBS assemblage are in keeping with terminal Pleistocene/early Holocene assemblages from other sites in the surrounding region, consistent with the OSL ages obtained from the LBS and PIT1 samples (Orton, 2006, Mackay et al., 2015, Mackay et al., 2019).

LGSS

LGSS provides the smallest sample of stone artefacts in the sequence (*n*=327), but is the uppermost stratum to underlie the black crust, and thus likely pre-dates ~57 ka (OSL1). Proportions of hornfels comparable to LBS suggest linkages to the Doring River; however, LGSS also has the highest proportion of silcrete of the strata under consideration. A single backed artefact was recorded, along with a complex notched 'strangulated' blade comparable to distinctive notched pieces from nearby Howiesons Poort contexts (Porraz et al., 2013, Mackay, 2010). Platform faceting on 14% of plotted flakes (18/127) confirms a largely MSA assemblage, as does the presence of small numbers of discoidal (*n*=2) and Levallois (*n*=1) cores. This is consistent with Parkington's observations on assemblages below the black crust. Bipolar cores are very common however (*n*=11), and the OSL ages from this part of the deposit show sediment mixing with MIS 1, 2, and 3 components (OSL4). LGSS thus appears to relate to the Howiesons Poort with some intrusive LSA material, potentially following sustained reoccupation of this part of the shelter after a ~45 kyr hiatus.

BS

The stone artefact assemblage from BS comprises 691 pieces. This is the youngest stratum in which quartzite is the dominant lithology, though proportions of silcrete and hornfels remain elevated. Five artefacts confidently classified as backed pieces were plotted, and a further two classified as possible backed pieces. Two of the notched artefacts were described as consistent with Howiesons Poort notched pieces. No bifacial points or thinning flakes were observed during classification of the BS assemblage; however, three unifacial points were found, two of which were made from silcrete and one from quartzite (Fig. 8 vii). Discoidal, rotated (or multiplatform), and bipolar cores are the three most common types identified, though Levallois forms are represented. These include a single 'Nubian-like' core associated with the early post-Howiesons Poort at Mertenhof (Fig. 8 ii), and at open sites in the region (Hallinan and Shaw, 2020, Will et al., 2015). The Nubian-like core and unifacial points all occur towards the top of BS in Square 2 where it is not overlain by LGSS, immediately below the age of 57 ± 3 ka (OSL1). Stratum BS also has an unusual prevalence of silcrete cores, accounting for 20.6% of the core total, as opposed to <10% for all the other MSA-assigned strata. Most of the stone artefacts in BS appear to relate to the Howiesons Poort, and the OSL samples for this unit would suggest that it largely formed during the earliest phases of that technocomplex.

GGLBS

In total, 507 artefacts were plotted in GGLBS, dated to ~85 ka. Assemblage composition is appreciably different from BS. Silcrete is uncommon, and quartzite is the dominant lithology. Sandstone—of which the shelter is composed—also becomes a substantial assemblage component. Denticulates (*n*=8) and notched pieces (*n*=7) are the most common implement types, and a single quartzite unifacial point was recorded. Around two-thirds of all cores were made from rock available in the immediate vicinity of the shelter, though another 23.5% were made from a decaying white stone that might previously have been hornfels (Will et al., 2015). Data available from O'Driscoll's more detail analysis of artefacts in this unit suggests high proportions of convergent flakes and of blades (Table 9); more than a quarter of all complete flakes in GGLBS had a convergent morphology. Three of the eight denticulates in GGLBS were made on convergent blanks (e.g., Fig. 8 xxiv).

PBS

PBS presents the largest sample in the sequence, comprising 2953 plotted artefacts. Quartzite remains common, but unlike all other units, sandstone is the most common lithology among artefacts. Between them, quartzite and sandstone account for 91.3% of the assemblage total; adding locally available quartz brings the total to 95.1%. Reinforcing the inference that raw material acquisition was principally local in PBS is the presence of a large (0.68 m) fragment of roof fall
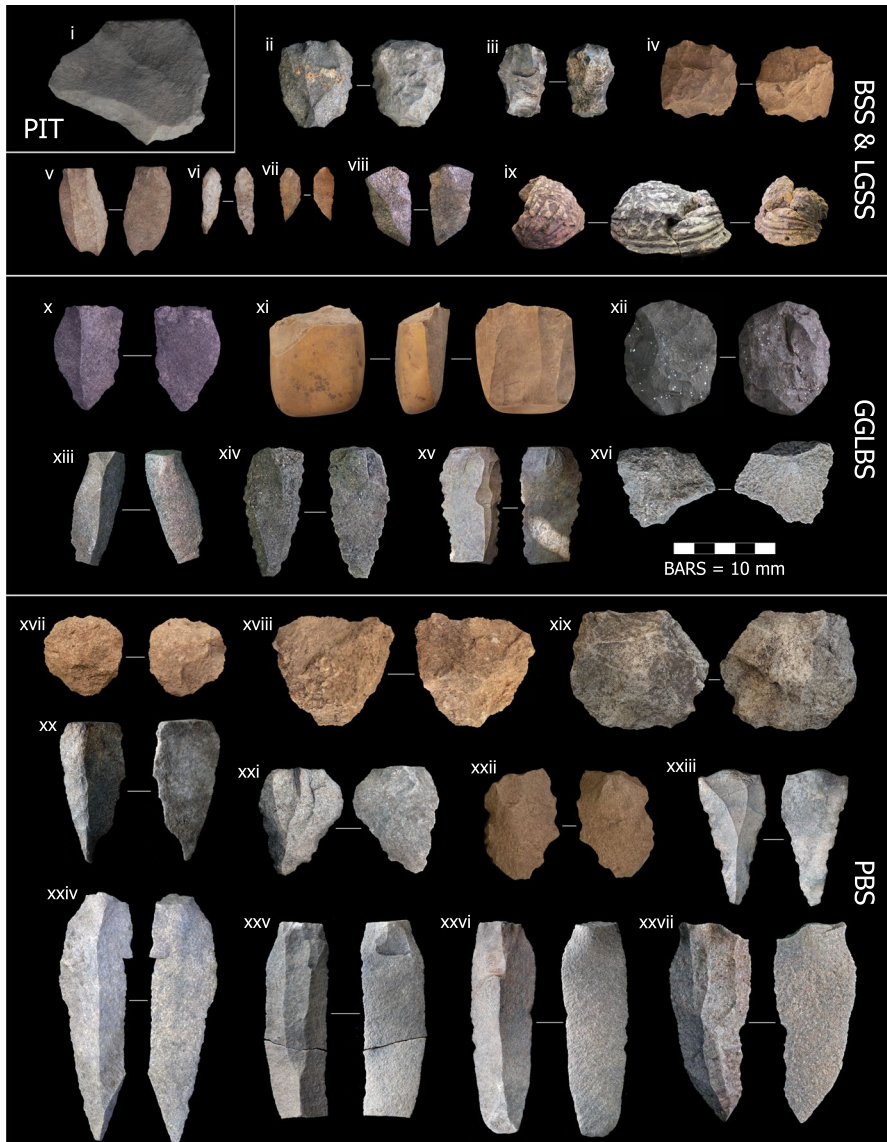
Fig. 8 Selection of stone artefacts from various layers. <u>PIT</u>: i. Large quartzite scraper found in base of pit near ochred grindstone. <u>BSS & LGSS</u>: ii. 'Nubian'-like preferential Levallois core, quartzite. iii. Opposed platform recurrent Levallois core, chert. iv. Recurrent Levallois, quartzite. v. Laminar flake, silcrete, with lateral damage, possibly use or fine retouch. vi. Bladelet, quartz. vii. Backed artefact, silcrete. viii. 'Tongati'-like unifacial point, quartzite, with invasive retouch on left lateral and marginal retouch on right lateral. ix. Trilobite. <u>GGLBS</u>: x. Convergent flake, quartzite. xi. Prepared core with laminar removals, hornfels. xii. Recurrent Levallois core, quartzite. xiii. Canted blade, quartzite. xiv. Denticulate on convergent blank, quartzite. xv. Denticulate, hornfels, broken. xvi. Notched flake, quartzite. <u>PBS</u>: xvii. Recurrent Levallois core, sandstone. xviii. 'Other prepared' core, sandstone. xix. Discoid, quartzite. xx. Unifacial point with invasive retouch down right lateral. xxi. Denticulate on convergent blank, quartzite. xxii. Denticulate on flake blank, quartzite. xxiii. Denticulate on convergent blank, hornfels. xxiv. Blade, quartzite. xxv. Blade, quartzite, broken. xxvi. Blade, quartzite. xxvii. Convergent flake, quartzite

Fig. 9 South section of Trench 1 showing piece plotted artefacts from GGLBS (blue) and PBS (green); conjoin sets presented as red lines
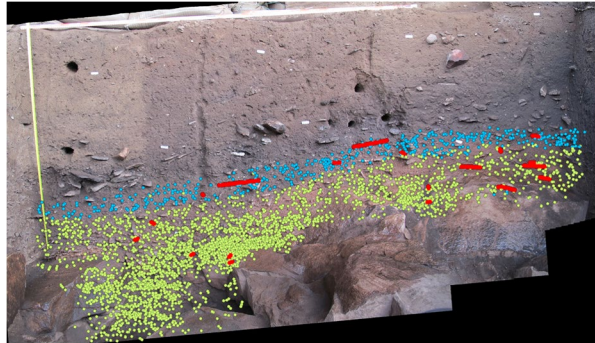
flaked heavily around one margin, and located towards the base of the deposit (Fig. 4F).

As with GGLBS, denticulates (*n*=66) and notched pieces (*n*=24) are the most common implement types, but unlike the overlying layer the former outnumber the latter considerably. Three unifacial points were also identified in PBS. PBS has a large sample of cores, though many (*n*=36) could not be classified to type. Discoidal cores are the most common identified type, followed by rotated cores. Consistent with the general raw material data, 93.2% of cores were made on rocks available in the vicinity of the shelter.

A final notable component of the PBS assemblage is the presence of blades over 80 mm (Fig. 8, #s 24–26), the largest having an axial length of 117.7 mm. Blades of comparable size do not occur in the overlying strata, and nor do these blades appear to have been produced from the cores in PBS, on which blade scars were uncommon.

Conjoins

No dedicated effort was made to identify refits or conjoins during cataloguing of KFR1; however, O'Driscoll identified a total of 42 conjoining broken artefact fragments comprising 19 conjoin sets during analysis of GGLBS and PBS (Fig. 9). The maximum distance between conjoining artefacts was 0.52 m, with an average distance of 0.11 m (calculated using the *philentropy* package in R (Drost, 2018)). All 19 sets fall within their respective stratigraphic units, and typically follow the dip of those units. Notably, though, the conjoins sets in the deepest part of PBS—corresponding to the bedrock cavity in Square 2—are typically more steeply aligned, albeit also typically closer together.

Fabric Analysis

In total, 752 artefacts were plotted with two or more points during excavations. Of these, artefacts with an elongation value of ≥1.6 can be used to generate a fabric
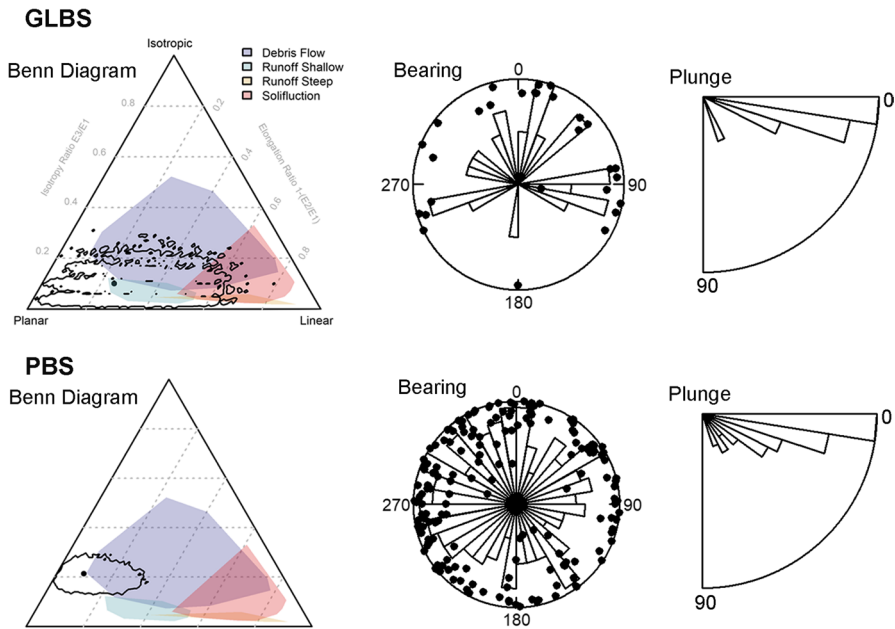
Fig. 10 Benn diagrams, bearing, and plunge results from two point shots for GGLBS and PBS

analysis for the sequence (Wilkins et al., 2020, Lenoble and Bertran, 2004, McPherron, 2018). As only the artefacts from the lowest two strata have so far been measured, allowing calculation of elongation, the available sample comprises 360 pieces, 50 of which come from GGLBS, and 310 from PBS (Fig. 10). The fabric analysis was conducted using the methods and R-code produced by McPherron (2018).

The small GGLBS sample has a large confidence interval that overlaps with expectations of shallow run-off and debris flow. The larger PBS sample is more strongly isotropic and has a confidence interval that overlaps with debris flow. In interpreting these results it needs to be borne in mind that the slope of the lowest deposits is quite variable due to the complex underlying topography of the bedrock. Isotropy may thus be exaggerated by variable depositional planes in the near-basal deposits. It is also possible that the general rear-to-front slope of the basal rock has led to some downslope movement of sediments and artefacts towards the front of the shelter, and this may explain the lack of early MSA towards the rear of the shelter.

Ochre

Pigments are reasonably common throughout the sequence at KFR1, occurring in all strata (Table 10). These typically take the form of iron-rich shales likely sourced from the nearby Bokkeveld Formation, but also include dense ironstone pieces that may come from further east in the Karoo. The total plotted sample is 183 pieces,

Table 10 Frequency of unworked and worked pigments

Stratum	Unworked	Worked	Total
LBS	18	3	21
LGSS	31	0	31
BS	35	3	38
GGLBS	39	5	44
PBS	35	8	43
Total	158	19	177

Fig. 11 Three faces of the deepest work ochre piece from KFR1. Ground (striated) face shown on left

around 10% of which show signs of working in the form of striated grinding facets with uni- or multi-directional grooves (Hodgskiss, 2010). No scored or engraved pieces were recovered. The deepest worked piece is a heavy fragment of ironstone with uni-directional parallel grooves on a single grinding facet (Fig. 11), located 0.36 m below the age of 166 ± 13 ka (OSL8).

Trilobite

A singular find in the KFR1 sequence is the endocast of an homalonotid trilobite of the genus *Burmeisteria* in unit BS (Figs. 4E and 8 ix). The fossil was located below the black crust in the south section of Square 1. Though the crust here is discontinuous, there are no organic items in the vicinity of the trilobite. An OSL sample (OSL12) taken at the find location provides an age of 69 ± 3 ka, supported by adjacent sample OSL14 (70 ± 5 ka), each with a minor secondary component dating to MIS 2. However, OSL13 gave a much older age of 87 ± 5 ka, consistent with those obtained from the underlying unit GGLBS. OSL15, taken just above the fossil location in unit LBS, demonstrated mixing between sediments dated to ~70 ka (37%), ~20 ka (~44%), and ~8 ka (19%). Given that (a) the lithics surrounding the trilobite are consistent with the Howiesons Poort, (b) the OSL age taken from

the find location dates to MIS 4, and (c) there are no organic items such as bone and shell around the find, it seems reasonable to assign a Howiesons Poort attribution to the find.

Burmeisteria fossils are common in the lower Bokkeveld Group shales (Cooper, 1982), which as noted earlier are exposed 400 m to the east of KFR1, but do not occur within the Nardouw Formation rocks which comprise the shelter itself. The trilobite was thus introduced to the site, potentially from relatively close by. While the find is the only one of its kind at KFR1, a *Burmeisteria* fossil has previously been reported from the dripline of another Cederberg rock shelter site, OP10, though this example was found on the surface and thus lacks context (Miller et al., 1991). Helm et al. (2019) report another trilobite find from the site of Cave 17 on the Robberg Peninsula, approximately 470 km to the south east of KFR1. As with OP10, the Cave 17 trilobite was recovered from the surface in a mixed lag assemblage. Interestingly, though, the description of that surface assemblage—"A variety of segments are present; bladelets, bladelet cores, and scrapers, of an average size (>40 mm), along with large flake blades and triangular flakes/blanks, 60–70 mm in length"—is more consistent with a Howiesons Poort association than with any other part of the known southern African sequence (Lombard et al., 2022).

Discussion and Conclusions

The deposits at KFR1 are deeper and older than expected based on Parkington's original excavation. Geophysics suggest a narrow band of deep deposits stretching across the centre of the site from south-west to north-east. None of these deep deposits occur in areas excavated to bedrock during 1969. Square 2 of the renewed excavations intersected the deepest sediments, but other areas of significant depth remain between our two excavation trenches (Fig. 6). Based on these results, we do not anticipate appreciably older deposits occurring in as-yet unsampled areas of the site, but it may be possible to increase the sample of deepest material which we only recovered from the cavity at the base of Square 2.

OSL and prior radiocarbon dating results suggest that KFR1 was occupied discontinuously from MIS 6 into the mid-Holocene, though the locus of occupation within the shelter appears to have shifted through time. Initial phases of occupation in MIS 6 and MIS 5 are concentrated towards the front of the shelter, while MIS 4 occupation associated with the Howiesons Poort was identified in both Trench 1 and in the previously reported Trench 2 towards the rear of the site (Mackay et al., 2019). There is very little evidence for occupation of KFR1 during MIS 3 (57–29 ka), something common to many sites in the surrounding region (Mitchell, 2008). The black crust appears to have formed across the front of the shelter during this time, consistent with crusts that formed during depositional hiatuses at other sites in the region (Ames et al., 2020, Volman, 1981). Interestingly, though, there is no comparable horizon marker for the ~70 kyr gap between PBS and GGLBS. Trampling and fragmentation of the crust with reoccupation of the cave in MIS 2 may explain the post-depositional mixing suggested in the OSL results, the apparent mixing of LSA and uppermost MSA artefacts, and the incorporation of small quantities

of bone and OES into the uppermost MSA strata. During early MIS 1, occupation was again concentrated towards the front of the shelter, with no signal post-13 ka in Trench 2. The OSL dating results from LBS confirm the radiocarbon date reported by Nackerdien (1989) for the base of the LSA in Parkington's original excavation.

Within the lowest three stratigraphic units there is little evidence for significant palaeoecological change despite the position of KFR1 near the modern boundary of the Fynbos and Succulent Karoo biomes, and despite those units spanning ~100 kyr including two glacials and an inter-glacial. This most likely reflects edaphic controls on the distribution of fynbos taxa (Carr et al., 2016, Esler et al., 2015, Richards et al., 1997), and the noted resistance of Cederberg flora to community-level turnover (Meadows and Sugden, 1993).

Distinctions between the front and rear trenches are not only occupational but also stratigraphic. The primary challenge faced by Parkington, and again in our re-excavation, was determining stratigraphic boundaries. This was not a problem in Trench 2, where stratigraphy was clearly visible. The difference is not a product of age: the Trench 2 deposits are all older than LBS in Trench 1 but more finely stratified. As noted in our report on Trench 2, however, stratigraphic resolution diminishes rapidly with distance from the rear wall, such that strata that were visible at the rear wall were not discernible 2 m closer to the shelter mouth. The visibly homogeneous nature of the Trench 1 sediments that Parkington commented on in 1969 is a continuation of this process. The causes of this are unknown but we can speculate that root activity associated with the greater soil moisture available towards the front of the site may have acted to redistribute sediments at small scales. The resulting presence of organic acids from root exudate (Adeleke et al., 2017) may also explain the loss of organic items like bone despite the neutral to alkali sediments.

Mapping of sedimentary boundaries and piece-plotted data allow us to overcome some of the stratigraphic challenges encountered by Parkington, but the deposit remains coarsely resolved and there is mixing, most notably at the contact between the MSA and LSA in units LGSS and LBS. KFR1 is unlikely ever to produce a 'clean', high-resolution sequence of behavioural or ecological change. Despite these limitations, the site usefully contributes to our understanding of the MSA. Though widely known as a 'Howiesons Poort site', that part of the sequence may be among the least interesting. Its main contributions in that respect are the presence of a trilobite suggesting acquisition and transport of presumably non-utilitarian items, and the surprisingly low density of artefacts; Howiesons Poort layers at sites in the surrounding region typically show intensive occupation (Miller et al., 2013, Mackay, 2010, Karkanas et al., 2015, Will et al., 2015). Artefact densities are lower in the earliest Howiesons Poort layers at Diepkloof and Klein Klipuhis (Mackay, 2009), however, and it may be that KFR1 was occupied in that interval.

Volman's MSA 2b sample from KFR1 is replicated in GGLBS and PBS, though these two units appear to have been deposited ~70 kyr apart. In our re-excavation, GGLBS and PBS have some different technological characteristics, the former more in keeping with MIS 2b, the latter having unresolved affinities. It is worth noting that Parkington's sample of PBS—taken as Spits 8 and 9—was quite small, and may have produced an ambiguous signal when aggregated with GGLBS. This aside, the artefacts from PBS warrant detailed further study, given

their antiquity and the presence of distinctive items including numerous denticulates and large blades. The ground ochre from PBS is currently among the oldest in southern Africa, particularly given that the deepest example occurred 0.36 m lower than the age of 166 ± 13 ka for OSL8.

A final note concerns the difficulties faced in reconstructing human behaviour in the earlier parts of the MSA. Occupation of Diepkloof and Hollow Rock Shelter overlaps with occupation of KFR1 during GGLBS, but the nearest occupation horizon within error of the dates we have for PBS is at Pinnacle Point on the south coast, located 350 km to the southeast of KFR1 (Jacobs, 2010). Wurz (2020) reasonably asks whether the distinctive tool production strategies identified by Schmid et al. (2016) in the MSA 1 at Elands Bay Cave—the nearest early MSA site—are reproduced at KFR1. The answer appears to be 'no', but based on the current chronologies, occupation of these two sites does not overlap. In their review of southern Africa's dated sites Lombard et al. (2022) identify 23 sites with a central age that falls within MIS 4, 32 within MIS 5, and only nine within MIS 6. To put it another way, the number of localities known to be occupied per thousand years is more than an order of magnitude lower in MIS 6 (0.14 localities/kyr) than in MIS 4 (1.64 localities/kyr) complicating comparative analyses between older assemblages.

KFR1 exemplifies many of the challenges of resolving the earlier phases of southern Africa's MSA. Occupation of the site was more than simply discontinuous: it was more often unoccupied than occupied in the last ~160 kyr. And even when occupied, the traces are spatially segregated and in some cases ephemeral. The bifacial point recovered by Poggenpoel during Parkington's excavation remains the only trace of occupation of the site during the Still Bay, despite intensive occupation of Hollow Rock Shelter 2 km away, and numerous open air Still Bay sites in the Doring River catchment (Mackay et al., 2021). It is possible that some of this relates to the particular landscape context of KFR1, located as it is away from reliable water in a semi-arid region; however, the site appears to have been relatively well-used during MIS 6 and MIS 2. Ultimately, developing the archaeology of the earlier MSA, during which many distinctively human behaviours presumably emerged, requires above all else a substantial increase in our sample of extensively excavated and dated sites.

Data Availability All data used in this paper are available on request.

Declarations

Ethical Approval Not applicable.

Competing Interests The authors declare no competing interests.

References

Adeleke, R., Nwangburuka, C., & Oboirien, B. (2017). Origins, roles and fate of organic acids in soils: A review. *South African Journal of Botany, 108*, 393–406.

Aitken, M. J. (1998). *An introduction to optical dating: the dating of Quaternary sediments by the use of photonstimulated luminescence*. Oxford: Oxford University Press.

Ames, C. J. H., Gliganic, L., Cordova, C. E., Boyd, K., Jones, B. G., Maher, L., & Collins, B. R. (2020). Chronostratigraphy, site formation, and palaeoenvironmental context of Late Pleistocene and Holocene occupations at Grassridge Rock Shelter (Eastern Cape, South Africa). *Open Quaternary, 6*.

Bøtter-Jensen, L., McKeever, S. W. S., & Wintle, A. G. (2003). *Optically stimulated luminescence dosimetry*. Amsterdam: Elsevier.

Carr, A. S., Chase, B. M., & Mackay, A. (2016). Mid to Late Quaternary landscape and environmental dynamics in the Middle Stone Age of southern South Africa. In S. Jones & B. A. Stewart (Eds.), *Africa from MIS 6-2: Population dynamics and paleoenvironments*. Springer.

Chazan, M., Berna, F., Brink, J., Ecker, M., Holt, S., Porat, N., Thorp, J. L., & Horwitz, L. K. (2020). Archeology, environment, and chronology of the Early Middle Stone Age component of Wonderwerk Cave. *Journal of Paleolithic Archaeology, 3*, 302–335.

Conyers, L. B. (2013). *Ground-penetrating radar for archaeology*. Lanham.

Cooper, M. R. (1982). A revision of the Devonian (Emsian-Eiflian) Trilobita from the Bokkeveld Groups of South Africa. *Annals of the South African Museum, 89*, 1–174.

Cordova, C., & Scott, L. (2010). The potential of Poaceae, Cyperaceae, and Restionaceae phytoliths to reflect past environmental conditions in South Africa. *Palaeoecololgy of Africa, 30*, 107–133.

Cordova, C. E. (2013). C3 Poaceae and Restionaceae phytoliths as potential proxies for reconstructing winter rainfall in South Africa. *Quaternary International, 287*, 121–140.

Dahlin, T., & Zhou, B. (2004). A numerical comparison of 2D resistivity imagingwith 10 electrode arrays. *Geophysical Prospecting, 52*, 379–398.

Dalan, R. A., & Banerjee, S. K. (1998). Solving archaeological problems using techniques of soil magnetism. *Geoarchaeology, 13*, 3–36.

Duller, G. A. T. (2004). Luminescence dating of quaternary sediments: Recent advances. *Journal of Quaternary Science, 19*, 183–192. https://doi.org/10.1002/jqs.809

Duller, G. A. T. (2012). Improving the accuracy and precision of equivalent doses determined using the optically stimulated luminescence signal from single grains of quartz. *Radiation Measurements, 47*, 770–777. https://doi.org/10.1016/j.radmeas.2012.01.006

Drost, H.-G. (2018). Philentropy: Information theory and distance quantification with R. *Journal of Open Source Software, 3*.

Esler, K. J., Von Staden, L., & Midgley, G. F. (2015). Determinants of the Fynbos/Succulent Karoo biome boundary: Insights from a reciprocal transplant experiment. *South African Journal of Botany, 101*, 120–128.

Esteban, I., de Vynck, J. C., Singels, E., Vlok, J., Marean, C. W., Cowling, R. M., Fisher, E. C., Cabanes, D., & Albert, R. M. (2017). Modern soil phytolith assemblages used as proxies for paleoscape reconstruction on the south coast of South Africa. *Quaternary International, 434*, 160–179.

Esteban, I., Marean, C. W., Fisher, E. C., Karkanas, P., Cabanes, D., & Albert, R. M. (2018). Phytoliths as an indicator of early modern humans plant gathering strategies, fire fuel and site occupation intensity during the Middle Stone Age at Pinnacle Point 5-6 (south coast, South Africa). *PLoS One, 13*, e0198558.

Evans, U. (1994). Hollow Rock Shelter, a Middle Stone Age site in the Cederberg. *Southern African Field Archaeology, 3*, 63–73.

Fu, X., Li, B., Jacobs, Z., Jankowski, N. R., Cohen, T. J. & Roberts R. G. (2020). Establishing standardised growth curves (SGCs) for OSL signals from individual grains of quartz: A continental-scale case study. *Quaternary Geochronology, 60*, 101107. https://doi.org/10.1016/j.quageo.2020.101107

Galbraith, R. F., Roberts, R. G., Laslett, G. M., Yoshida, H., & Olley, J. M. (1999). Optical dating of single and multiple grains of quartz from Jinmium rock shelter, northern Australia: Part I, experimental design and statistical models. *Archaeometry, 41*, 339–364. https://doi.org/10.1111/j.1475-4754.1999.tb00987.x

Galbraith, R. F., & Roberts, R. G. (2012). Statistical aspects of equivalent dose and error calculation and display in OSL dating: An overview and some recommendations. *Quaternary Geochronology, 11*, 1–27. https://doi.org/10.1016/j.quageo.2012.04.020

Gliganic, L. A., Jacobs, Z., & Roberts, R. G. (2012). Luminescence characteristics and dose distributions for quartz and feldspar grains from Mumba rockshelter, Tanzania. *Archaeological and Anthropological Sciences, 4*, 115–135. https://doi.org/10.1007/s12520-011-0085-9

Goldberg, P., & Macphail, R. I. (2006). *Practical and theoretical geoarchaeology*. Blackwell Publishing.

Guo, Y.-J., Li, B., Zhang, J.-F., Yuan, B.-Y., Xie, F., & Roberts, R. G. (2017). New ages for the Upper Palaeolithic site of Xibaimaying in the Nihewan Basin, northern China: Implications for small-tool and microblade industries in northeast Asia during Marine Isotope Stages 2 and 3. *Journal of Quaternary Science, 32*, 540–552. https://doi.org/10.1002/jqs.2949

Hallinan, E., & Shaw, M. (2020). Nubian Levallois reduction strategies in the Tankwa Karoo, South Africa. *PLoS One, 15*, e0241068.

Helm, C. W., Benoit, J., Mayor, A., Cawthra, H. C., Penn-Clarke, C. R., & Rust, R. (2019). Interest in geological and palaeontological curiosities by southern African non-western societies: A review and perspectives for future study. *Proceedings of the Geologists' Association, 130*(5), 541–558.

Henshilwood, C. S. (2012). Late Pleistocene Techno-traditions in Southern Africa: A review of the Still Bay and Howiesons Poort, c. 75–59 ka. *Journal of World Prehistory, 25*, 205–237.

Hodgskiss, T. (2010). Identifying grinding, scoring and rubbing use-wear on experimental ochre pieces. *Journal of Archaeological Science, 37*, 3344–3358.

Högberg, A. (2014). Chronology, stratigraphy and spatial distribution of artefacts at Hollow Rock Shelter, Cape Province, South Africa. *South African Archaeological Bulletin, 69*, 142–151.

Högberg, A., & Larsson, L. (2011). Lithic technology and behavioural modernity: New results from the Still Bay site, Hollow Rock Shelter, Western Cape Province, South Africa. *Journal of Human Evolution, 61*, 133–155.

Hogg, A. G., Heaton, T. J., Hua, Q., Palmer, J. G., Turney, C. S. M., Southon, J., Bayliss, A., Blackwell, P. G., Boswijk, G., Bronk Ramsey, C., Pearson, C., Petchey, F., Reimer, P., Reimer, R., & Wacker, L. (2020). SHCal20 southern hemisphere calibration, 0–55,000 years cal BP. *Radiocarbon, 62*, 759–778.

Hu, Y., Marwick, B., Zhang, J. F., et al. (2019). Late Middle Pleistocene Levallois stone-tool technology in southwest China. *Nature, 565*, 82–85. https://doi.org/10.1038/s41586-018-0710-1

Hu, Y., Ruan, Q., Liu, J., Marwick, B., & Li, B. (2020). Luminescence chronology and lithic technology of Tianhuadong Cave, an early Upper Pleistocene Paleolithic site in southwest China. *Quaternary Research, 94*, 121–136. https://doi.org/10.1017/qua.2019.67

Huntley, D., Godfrey-Smith, D., & Thewalt, M. (1985). Optical dating of sediments. *Nature, 313*, 105–107. https://doi.org/10.1038/313105a0

Jacobs, Z. (2010). An OSL chronology for the sedimentary deposits from Pinnacle Point Cave 13B--a punctuated presence. *Journal of Human Evolution, 59*, 289–305.

Jacobs, Z., & Roberts, R. G. (2015). An improved single grain OSL chronology for the sedimentary deposits from Diepkloof Rockshelter, Western Cape, South Africa. *Journal of Archaeological Science, 63*, 175–192.

Jacobs, Z., Roberts, R. G., Galbraith, R. F., Deacon, H. J., Grun, R., Mackay, A., Mitchell, P., Vogelsang, R., & Wadley, L. (2008). Ages for the Middle Stone Age of southern Africa: Implications for human behavior and dispersal. *Science, 322*, 733–735.

Jacobs, Z., Li, B., Farr, L., Hill, E., Hunt, C., Jones, S., Rabett, R., Reynolds, T., Roberts, R. G., Simpson, D., & Barker, G. (2017). The chronostratigraphy of the Haua Fteah cave (Cyrenaica, northeast Libya) — optical dating of early human occupation during Marine Isotope Stages 4, 5 and 6. *Journal of Human Evolution, 105*, 69–88. https://doi.org/10.1016/j.jhevol.2017.01.008

Karkanas, P., Brown, K. S., Fisher, E. C., Jacobs, Z., & Marean, C. W. (2015). Interpreting human behavior from depositional rates and combustion features through the study of sedimentary microfacies at site Pinnacle Point 5-6, South Africa. *Journal of Human Evolution, 85*, 1–21.

Kreutzer, S., Schmidt, S., Fuchs, M. C., Dietze, M., Fischer, M., & Fuchs, M. (2012). Introducing an R package for luminescence dating analysis. *Ancient TL, 30*, 1–8.

Kreutzer, S., Burow, C., Dietze, M., Fuchs, M., Schmidt, C., Fischer, M., Friedrich, J., Mercier, N., Philippe, A., Riedesel, S., Autzen, M., Mittelstrass, D., & Gray, H. (2021). *Luminescence: Comprehensive luminescence dating data analysis.* R package version 0.9.15. https://CRAN.R-project.org/package=Luminescence

Lenoble, A., & Bertran, P. (2004). Fabric of Palaeolithic levels: Methods and implications for site formation processes. *Journal of Archaeological Science, 31*, 457–469.

Li, B., Jacobs, Z., & Roberts, R. G. (2016). Investigation of the applicability of standardised growth curves for OSL dating of quartz from Haua Fteah cave, Libya. *Quaternary Geochronology, 35*, 1–15. https://doi.org/10.1016/j.quageo.2016.05.001

Li, B., Jacobs, Z., Roberts, R. G., Galbraith, R., & Peng, J. (2017). Variability in quartz OSL signals caused by measurement uncertainties: problems and solutions. *Quaternary Geochronology, 41*, 11–25. https://doi.org/10.1016/j.quageo.2017.05.006

Li, B., Jacobs, Z., & Roberts, R. G. (2020). Validation of the LnTn method for De determination in optical dating of Kfeldspar and quartz. *Quaternary Geochronology, 58*, 101066. https://doi.org/10.1016/j.quageo.2020.101066

Loke, M. H., Chambers, J. E., Rucker, D. F., Kuras, O., & Wilkinson, P. B. (2013). Recent developments in the direct-current geoelectrical imaging method. *Journal of Applied Geophysics, 95*, 135–156.

Lombard, M., Bradfield, J., Caruana, M. V., Makhubela, T. T. V., Dusseldrop, G., & Wurz, S. (2022). The southern African Stone Age sequence updated (II). *South African Archaeological Bulletin, 77*.

Low, M. (2019). Continuity, variability and the nature of technological change during the Late Pleistocene at Klipfonteinrand Rockshelter in the Western Cape, South Africa. *African Archaeological Review, 36*(1), 67–88.

Mackay, A. (2009). *History and selection in the Late Pleistocene archaeology of the Western Cape, South Africa*. PhD, Australian National University.

Mackay, A. (2010). The Late Pleistocene archaeology of Klein Kliphuis rockshelter, Western Cape, South Africa: 2006 excavations. *South African Archaeological Bulletin, 65*, 132–147.

Mackay, A., Ames, C. J. H., McNeil, J.-L., & Shaw, M. (2021). Reconstructing Middle Stone Age mobility patterns from raw material transfers in South Africa's Still Bay (77–70 ka) technocomplex. *Archaeological and Anthropological Sciences, 14*.

Mackay, A., Armitage, S. J., Niespolo, E. M., Sharp, W. D., Stahlschmidt, M., Blackwood, A. F., Boyd, K., Chase, B. M., Lagle, S., Kaplan, C. K., LOW, M. A., Martisius, N. L., McNeil, P. J., Moffat, I., O'Driscoll, C. A., Rudd, R., Orton, J. D., & Steele, T. E. (2022a). Environmental influences on human innovation and behavioural diversity in southern Africa 92-80 000 years ago. *Nature Ecology and Evolution, 6*(4), 361–369.

Mackay, A., Armitage, S. J., Niespolo, E. M., Sharp, W. D., Stahlschmidt, M. C., Blackwood, A. F., Boyd, K. C., Chase, B. M., Lagle, S. E., Kaplan, C. F., Low, M. A., Martisius, N. L., McNeill, P. J., Moffat, I., O'driscoll, C. A., Rudd, R., Orton, J. D., & Steele, T. E. (2022b). Environmental influences on human innovation and behavioural diversity in southern Africa 92–80 Thousand years ago. *Nature Ecology & Evolution, 6*, 361–369.

Mackay, A., Cartwright, C., Heinrich, S., Low, M., Stahlschmidt, M., & Steele, T. E. (2019). Excavations at Klipfonteinrand reveal local and regional patterns of adaptation and interaction through MIS 2 in southern Africa. *Journal of Paleolithic Archaeology, 3*, 362–397.

Mackay, A., Jacobs, Z., & Steele, T. E. (2015). Pleistocene archaeology and chronology of Putslaagte 8 (PL8) rockshelter, Western Cape, South Africa. *Journal of African Archaeology, 13*, 71–98.

Mackay, A., Stewart, B. A., & Chase, B. M. (2014). Coalescence and fragmentation in the late Pleistocene archaeology of southernmost Africa. *Journal of Human Evolution, 72*, 26–51.

Mcpherron, S. P. (2018). Additional statistical and graphical methods for analyzing site formation processes using artifact orientations. *PLoS One, 13*, e0190195.

Meadows, M. E., & Sugden, J. M. (1993). The late Quaternary palaeoecology of a floristic kingdom: The southwestern Cape South Africa. *Palaeogeography, Palaeoclimatology, Palaeoecology, 101*, 271–281.

Miller, C. E., Goldberg, P., & Berna, F. (2013). Geoarchaeological investigations at Diepkloof Rock Shelter, Western Cape, South Africa. *Journal of Archaeological Science, 40*, 3432–3452.

Miller, D., Yates, R., Manhire, T., & Lanham, J. (1991). An early interest in fossils? *The Digging Stick, 8*, 2–3.

Mitchell, P. J. (2008). Developing the archaeology of Marine Isotope Stage 3. *South African Archaeological Society Goodwin Series, 10*, 52–65.

Morrissey, P., Mentzer, S. M., & Wurz, S. (2022). A critical review of the stratigraphic context of the MSA I and II at Klasies River Main Site. *South Africa. Journal of Paleolithic Archaeology, 5*.

Mucina, L., & Rutherford, M. C. (2006). *The vegetation of South Africa, Lesotho and Swaziland*. South African National Biodiversity Institute.

Murray, A. S., & Wintle, A. G. (2000). Luminescence dating of quartz using an improved single-aliquot regenerativedose protocol. *Radiation Measurements, 32*, 57–73.

Nackerdien, R. (1989). *Klipfonteinrand 2: A sign of the times*. University of Cape Town.

Neumann, K., Strömberg, C., Ball, T., Albert, R. M., Vrydaghs, L., & Cummings, L. (2019). International Code for Phytolith Nomenclature (ICPN) 2.0. *Annals of Botany, 124*, 189–199.

Orton, J. (2006). The Later Stone Age lithic sequence at Elands Bay, Western Cape, South Africa: Raw materials, artefacts and sporadic change. *Southern African Humanities, 18*, 1–28.

Parkington, J. (1980). Time and place: Some observations on spatial and temporal patterning in the Later Stone Age sequence in southern Africa. *South African Archaeological Bulletin, 35*, 73–112.

Parkington, J. E. (1977). *Follow the San. PhD Unpublished PhD thesis*. Cambridge University.

Peng, J., & Li, B. (2017). Single-aliquot regenerative-dose (SAR) and standardised growth curve (SGC) equivalent dose determination in a batch model using the R package "numOSL." *Ancient TL, 35*, 32–53.

Peng, J., Dong, Z. B., Han, F. Q., Long, H., & Liu, X. J. (2013). R package numOSL: Numeric routines for optically stimulated luminescence dating. *Ancient TL, 31*, 41–48.

Piperno, D. R. (2006). *Phytoliths: A comprehensive guide for archaeologists and paleoecologists*. AltaMira Press.

Porraz, G., Texier, P.-J., Archer, W., Piboule, M., Rigaud, J.-P., & Tribolo, C. (2013). Technological successions in the Middle Stone Age sequence of Diepkloof Rock Shelter, Western Cape, South Africa. *Journal of Archaeological Science, 40*, 3376–3400.

Powell, R., Hergt, J., & Woodhead, J. (2002). Improving isochron calculations with robust statistics and the bootstrap. *Chemical Geology, 185*, 191–204. https://doi.org/10.1016/S0009-2541(01)00403-X

R Core Team. (2020). R: A language and environment for statistical computing, Vienna, Austria. https://www.Rproject.org/

Reidsma, F. H., Sifogeorgaki, I., Dinckal, A., Huisman, H., Sier, M. J., Van Os, B., & Dusseldorp, G. L. (2021). Making the invisible stratigraphy visible: A grid-based, multi-proxy geoarchaeological study of Umhlatuzana Rockshelter, South Africa. *Frontiers in Earth Science, 9*.

Richards, M. B., Stock, W. D., & Cowling, R. M. (1997). Soil nutrient dynamics and community boundaries in the Fynbos vegetation of South Africa. *Plant Ecology, 130*, 143–153.

Richter, D., Grun, R., Joannes-Boyau, R., Steele, T. E., Amani, F., Rue, M., Fernandes, P., Raynal, J. P., Geraads, D., Ben-Ncer, A., Hublin, J. J., & McPherron, S. P. (2017). The age of the hominin fossils from Jebel Irhoud, Morocco, and the origins of the Middle Stone Age. *Nature, 546*, 293–296.

Roberts, R. F., Jacobs, Z., Li, B., Jankowski, N. R., Cunningham, A. C., & Rosenfeld, A. B. (2015). Optical dating in archaeology: Thirty years in retrospect and grand challenges for the future. *Journal of Archaeological Science, 56*, 41–60. https://doi.org/10.1016/j.jas.2015.02.028

Rousseeuw, P. J., Debruyne, M., Engelen, S., & Hubert, M. (2006). Robustness and outlier detection in chemometrics. *Critical Reviews in Analytical Chemistry, 36*, 221–242. https://doi.org/10.1080/10408340600969403

Samouëlian, A., Cousin, I., Tabbagh, A., Bruand, A., & Richard, G. (2005). Electrical resistivity survey in soil science: A review. *Soil and Tillage Research, 83*, 173–193.

Sampson, C. G. (1974). *The Stone Age archaeology of southern Africa*. Academic Press.

Scerri, E. M. L., & Will, M. (2023). The revolution that still isn't: The origins of behavioral complexity in Homo sapiens. *Journal of Human Evolution, 179*, 103358.

Schmid, V., Conard, N. J., Parkington, J., Texier, P. J., & Porraz, G. (2016). The 'MSA 1' of Elands Bay Cave (South Africa) in the context of the southern African Early MSA technologies. *Southern African Humanities, 29*, 153–201.

Scott, L., Manzano, S., Carr, A. S., Cordova, C., Ochando, J., Bateman, M. D., & Carrión, J. S. (2021). A 14000 year multi-proxy alluvial record of ecotone changes in a Fynbos-Succulent Karoo transition in South Africa. *Palaeogeography, Palaeoclimatology, Palaeoecology, 569*.

Thackeray, A. I. (1977). *Stone artefacts from Klipfonteinrand*. University of Cape Town.

Thomsen, K. J., Murray, A. S., Buylaert, J. P., Jain, M., Hansen, J. H., & Aubry, T. (2016). Testing single-grain quartz OSL methods using sediment samples with independent age control from the Bordes-Fitte rockshelter (Roches d'Abilly site, Central France). *Quaternary Geochronology, 31*, 77–96. https://doi.org/10.1016/j.quageo.2015.11.002

Tribolo, C., Mercier, N., Valladas, H., Lefrais, Y., Miller, C., Parkington, J., & Porraz, G. (2016). Chronology of the Pleistocene deposits at Elands Bay Cave (South Africa) based on charcoals, burnt lithics, and sedimentary quartz and feldspar grains. *Southern African Humanities, 29*, 129–152.

Volman, T. P. (1981). *The Middle Stone Age in the Southern Cape*. PhD, University of Chicago.

Wadley, L. (2015). Those marvellous millennia: the Middle Stone Age of Southern Africa. *Azania: Archaeological Research in Africa, 50*, 155–226.

Wilkins, J., Schoville, B. J., Brown, K. S., Gliganic, L., Meyer, M. C., Loftus, E., Pickering, R., Collins, B., Blackwood, A. F., Makalima, S., Hatton, A., & Maape, S. (2020). Fabric analysis and chronology at Ga-Mohana Hill North Rockshelter, Southern Kalahari Basin: Evidence for in situ, stratified Middle and Later Stone Age deposits. *Journal of Paleolithic Archaeology, 3*, 336–361.

Will, M., & Conard, N. J. (2018). Assemblage variability and bifacial points in the lowermost Sibudan layers at Sibudu, South Africa. *Archaeological and Anthropological Sciences, 10*, 389–414.

Will, M., Mackay, A., & Phillips, N. (2015). Implications of Nubian-like core reduction systems in Southern Africa for the Identification of early modern human dispersals. *PLoS One, 10*, e0131824.

Wintle, A. G. (1997). Luminescence dating procedures and laboratory protocols. *Radiation Measurements, 27*, 769–817. https://doi.org/10.1016/S1350-4487(97)00220-5

Wintle, A. G. (2014). Luminescence dating methods. In H. Holland, & K. Turekian (Eds.), *Treatise on geochemistry* (2nd edn., vol. 14, pp. 17–35). Oxford: Elsevier. https://doi.org/10.1016/B978-0-08-095975-7.01203-1

Wurz, S. (2020). The Early Middle Stone Age in South Africa. *Oxford Research Encyclopedia of Anthropology*. https://doi.org/10.1093/acrefore/9780190854584.013.118

Zhang, D., Xia, H., Chen, F., Li, B., Slon, V., et al. (2020). Denisovan DNA in late Pleistocene sediments from Baishiya Karst cave on the Tibetan Plateau. *Science, 370*, 584–587. https://doi.org/10.1126/science.abb6320

Authors and Affiliations

Alex Mackay[1,2,3] ⬤ · **Rosaria B. K. Saktura**[1] ⬤ · **Corey A. O'Driscoll**[1] ⬤ ·
Kelsey C. Boyd[1] ⬤ · **Ben Marwick**[4] ⬤ · **Ian Moffat**[5] ⬤ · **Zenobia Jacobs**[1,3] ⬤

✉   Alex Mackay
     amackay@uow.edu.au

1   Centre of Archaeological Science, School of Earth, Atmospheric and Life Sciences, University
     of Wollongong, Wollongong, New South Wales 2522, Australia

2   Department of Archaeology, University of Cape Town, Cape Town, Western Cape 8001,
     South Africa

3   ARC Centre of Excellence for Australian Biodiversity and Heritage & Centre for Archaeological
     Science, School of Earth, Atmospheric and Life Sciences, University of Wollongong,
     Wollongong, New South Wales 2522, Australia

4   Department of Anthropology, University of Washington, Seattle, WA 98195, USA

5   Archaeology, College of Humanities, Arts and Social Sciences, Flinders University, Adelaide,
     South Australia 5001, Australia